Summer 8-23-2019

Dynamic Regulation of G-Protein Signaling

William C. Simke
University of Maine, william.simke@maine.edu

DYNAMIC REGULATION OF G-PROTEIN SIGNALING

By

William C. Simke

B.S. University of Maryland Baltimore County, 2016

A THESIS

Submitted in Partial Fulfillment of the

Requirements for the Degree of

Master of Science

(in Biochemistry)

The Graduate School

The University of Maine

August 2019

Advisory Committee:

Joshua B. Kelley, Assistant Professor of Biochemistry, Advisor

Dorothy E. Croall, Professor of Biochemistry

Robert E. Gundersen, Associate Professor of Biochemistry and Chair of Molecular and Biomedical Sciences

DYNAMIC REGULATION OF G-PROTEIN SIGNALING

By William C. Simke

Thesis Advisor: Dr. Joshua Kelley

An Abstract of the Thesis Presented
In Partial Fulfillment of the Requirements for the
Degree of Master of Science
(in Biochemistry)
August 2019

G protein-coupled receptors (GPCRs) are involved in numerous signaling processes ranging from neuronal growth to immune cells tracking invaders. GPCR signaling plays a role in many human diseases and thus GPCRs are important drug targets. Yeast respond to mating pheromone using a GPCR signaling system homologous to those used in humans to polarize their cytoskeleton toward the pheromone source. This is accomplished by initializing a MAPK signaling cascade to arrest the cells in mitosis and upregulate expression of chemotropic proteins. Pathway desensitization is accomplished by the Regulator of G-protein Signaling (RGS). RGS abrogates signaling by binding to the active GPCR, accelerating hydrolysis of GTP bound to G-proteins, bringing them to an inactive state. Previous studies have found the yeast RGS, Sst2, undergoes feedback phosphorylation by the MAPK, though the effect of this modification on RGS function was not determined. We examined the spatiotemporal dynamics of Sst2 using fluorescent live cell imaging in a microfluidics gradient chamber and performed computational image analysis of single cells. We have found that changes in Sst2 localization during the pheromone response are controlled by phosphorylation, removing Sst2 from regions of barrier proteins, known as septins. Furthermore, our data suggests that this phosphorylation event in turn changes the localization

of the MAPK. We show that the formin Bni1 is the pheromone responsive formin and is required for endocytic rates to be maintained during chemotropic growth. Finally, we provide evidence that the defects observed in endocytosis may be due to the improper localization of Gα bound MAPK. These results provide insight into previously unknown regulatory roles of the RGS during the yeast pheromone response.

ACKNOWLDGEMENTS

I'd like to thank my family for all their support and encouragement in helping me achieve my goals. I would especially like to thank my Grandma, Oma, and Opa for encouraging me to explore the natural world. A big thanks to Josh and my peers for all they have taught me in pursuit of this degree.

TABLE OF CONTENTS

LIST OF TABLES

LIST OF FIGURES

CHAPTER 1

INTRODUCTION

1.1 Background

Cells respond to a myriad of stimuli ranging from nutrient availability to the presence of cells in their surroundings by using transmembrane receptors to sense the external environment. The largest class of receptors that enable this sensing of the environment is the G-protein Coupled Receptor (GPCR) family (Sriram 2018). Examples in humans range from the olfactory receptors (Buck and Axel 1991), giving us the ability to smell, to acetylcholine receptors (Berrie et al. 1979), allowing proper communication throughout the brain and body. The budding yeast, Saccharomyces cerevisiae, contains two GPCRs, one to sense the availability of glucose and the other to find a mating partner (Versele, Lemaire, and Thevelein 2001; Kraakman et al. 1999). When attempting to mate, yeast will polarize and grow towards the mating partner, tracking the external gradient of signal in a process called chemotropism (Alvaro and Thorner 2016).

The study of the dynamics of G-Protein signaling is commonly performed in yeast, due to their conserved signaling pathways to that in humans, as well as their easy maintenance and manipulation (Dohlman et al. 1991). The haploid form of yeast is a useful model organism due to its genotype, in which only there is only one set of genes. This allows the manipulation of the genome, by means of fusing a fluorescent or epitope tag to the protein, or through the introduction of mutations with relative ease, as yeast are able to readily recombine foreign

DNA into their genome without the use of restriction enzymes or more complex methods such as CRISPR Cas9 (Gardner and Jaspersen 2014).

Yeast can stably exist as either a haploid or diploid. In the haploid form there are two mating types, MATa and MATα, which mate to form the diploid yeast (Herskowitz 1988; Haber 2012). For the haploid cells to reach the diploid form, each mating type secretes a mating pheromone, a short oligopeptide, which binds the opposite mating types pheromone responsive GPCR (Caldwell, Naider, and Becker 1995). The MATa cells, which bind α factor, are commonly used as the preferred mating type to work with, due to the higher solubility of α-factor compared to that of a-factor. Upon binding the mating pheromone, the cells initiate an internal signaling response, promoting a reorganization of the cytoskeleton and growth towards the source of pheromone (Segall 1993; Arkowitz 2009; Alvaro and Thorner 2016). In order for the yeast to accurately find the opposite mating type, they track a pheromone gradient, sensing in which direction the highest concentration of pheromone lies (Arkowitz 2009; Dyer et al. 2014; Alvaro and Thorner 2016). Unlike mammalian cells which are comparatively large, ranging in the tens of micrometers, yeast cells on average measure 5 microns in diameter. This small size means the concentration of pheromone on one side of the yeast to the other varies by a small amount, resulting in the difference in activation of about 1% of total receptors, a small number to accurately and readily determine where the higher source of pheromone is originating from (Segall 1993). Despite this difficulty, yeast are capable of tracking very shallow gradients (Dyer et al. 2014). Regardless of the spatial character of the extracellular signal, yeast are able to polarize their cellular machinery to a single point on the periphery of the cell, known as the polar cap (Slaughter, Smith, and Li 2009; McClure et al.

2015). Here, both receptors and downstream effectors in the pheromone response are concentrated to a mobile spot that can sample the signal at different places on the surface of the cell and eventually find the part of the yeast experiencing the highest signal (McClure et al. 2015, Alvaro and Thorner 2016).

Activation of the pheromone receptor, Ste2, is initiated by the binding of the mating pheromone, α-factor, which activates a heterotrimeric G-Protein (Wang and Dohlman 2004). The ligand bound receptor then acts as a Guanine nucleotide Exchange Factor (GEF) promoting exchange of GDP for GTP on the Gα subunit, Gpa1, and its dissociation from the Gβγ heterodimer, Ste4/Ste18, resulting in two active signaling pathways (Wang and Dohlman 2004; Dohlman and Thorner 2001; Alvaro and Thorner 2016). Free Gβγ is able to recruit scaffolding proteins and kinases to sites of active signaling, initiating two downstream pathways: 1) a Mitogen Activated Protein Kinase (MAPK) signaling cascade that results in transcription of mating genes and arrest of the cell cycle in the G1 phase, and 2) activation of the Rho family member Cdc42 that results in formation of the polar cap (Leberer et al. 1992; Nern and Arkowitz 1999). Active Cdc42 controls cytoskeletal reorganization and contributes to the initiation of the MAPK cascade(Figure 1A) (Bi and Park 2012).

Cdc42 is activated by the GEF, Cdc24, which is recruited to sites of active Gβγ by the factor arrest protein, Far1 (Shimada, Gulli, and Peter 2000; Butty et al. 2002; Nern and Arkowitz 1999). Once activated, Cdc42 in conjunction with Gic1 recruit and polymerize septins at the base of the forming shmoo to form a physical and biochemical barrier for the wandering polarity patch (Sadian et al. 2013; Kelley et al. 2015). Proper septin deposition is controlled by the Rho GTPase Accelerating Proteins (GAPs), Bem3, Rga1, and Rga2, which are recruited to

Cdc42 to hydrolyze bound GTP to Cdc42 and terminate its signaling (Caviston et al. 2003; Smith et al. 2002).The final MAPK in the MAPK cascade, Fus3, alters transcriptional output in the nucleus by silencing inhibitors and turning on activating factors through phosphorylation (Elion, Satterberg, and Kranz 1993; Hao et al. 2008; Alvaro and Thorner 2016). Additionally, Fus3 is recruited to active Gα, phosphorylating multiple substrates at the polarity patch to allow proper shmoo formation and growth (Metodiev et al. 2002; Errede et al. 2015). The formin Bni1, an actin nucleating protein, is activated through a two-step process in which Cdc42 binds, abrogating autoinhibition and allowing phosphorylation by Fus3, to complete the activation(Matheos et al. 2004; Evangelista et al. 1997). Active Bni1 nucleates actin cables in an Arp2/3 independent manner, allowing filament formation and condensation of the polarisome, bringing active subunits in close proximity to one another allowing the maintenance of signaling (Buttery, Yoshida, and Pellman 2007; Moseley et al. 2004; Goode, Eskin, and Wendland 2015; Karpova et al. 1998).

As the process of tracking pheromone is highly dynamic, negative regulation of the pheromone pathway is required to allow proper chemotropic growth toward the pheromone source. The main negative regulator of G-Protein Signaling (RGS), Sst2, was discovered in yeast nearly 20 years ago and acts as a GAP to the GTP-bound Gα subunit(Dohlman and Thorner 1997; Dohlman et al. 1996). Since the discovery of Sst2, the RGS family has been found to include homologs and orthologs across eukaryotes with varying function (Gold et al. 1997; Dohlman and Thorner 1997). In yeast, the RGS binds active receptor through its DEP (Disheveled, Egl-10, Pleckstrin) domain and quenches signaling through accelerating GTP hydrolysis on the Gα subunit. The GDP bound Gα subunit re-associates with the heterotrimeric

G-Protein(Dohlman and Thorner 1997; Ballon et al. 2006). Interestingly, it has been found that Sst2 contains a proline-directed phosphorylation site at serine 539 and that it is phosphorylated by Fus3 during the pheromone response (Garrison, Apanovitch, and Dohlman 2002; Tanaka and Yi 2010; Garrison et al. 1999). Initial studies using standard biochemical techniques found phosphorylation of Sst2 by Fus3 stabilizes Sst2, though the cellular process affected by this regulation is still unknown(Garrison et al. 1999; Garrison, Apanovitch, and Dohlman 2002). Interestingly, these initial studies found that there is no increase in pheromone sensitivity, even though the phosphorylation site lies in RGS domain of Sst2. These two observations guided our group to hypothesize that the phosphorylation site is necessary for the proper localization of Sst2. Additionally, it had been shown that Sst2 and septins cooperate to promote shmooing, through the proper localization and deposition of septins (Kelley et al. 2015). Furthermore, it has been shown through yeast two hybrid assays, that Sst2 physically interacts with the formin Bnr1 and the kelch-repeat protein, Kel1 (Burchett et al. 2002). This led us to pursue the hypothesis that Sst2 possesses previously unexplored binding interactions required for gradient tracking.

Kel1 has been shown to negatively regulate formins and mitotic exit, as well as associate with the endocytic protein, End3 (Gould et al. 2014; Whitworth et al. 2014; Hofken and Schiebel 2002; Raths et al. 1993). Yeast possess two formins, Bni1 and Bnr1, which are necessary to nucleate actin cables and are thought to have a redundant function in yeast. Interestingly, each of these formins localizes differentially during mitosis, with Bnr1 localizing to the bud neck only, and Bni1 localizing to sites of polarity. Regulation of the formin, Bnr1 is accomplished through a trimer composed of Kel1, Kel2, and the bud site selection protein, Bud14(Gould et al. 2014).

Although there is no direct linkage of Kel1 controlling the polarisome associated yeast formin, Bni1, it has been found that the S. pombe homologue of Bni1, for3p, is regulated by the Kel1 homologue, tea1 (Martin et al. 2005; Feierbach, Verde, and Chang 2004). Previous work that proved Kelch proteins and Bud14 form a large complex to negatively regulate Bnr1, noted that the localization of Kel1 was coincident to that of Bni1, localizing to sites of polarity (Gould et al. 2014). This observation led us to pursue the idea that Bni1 is regulated by Kel1 and that this interaction may be due in part to action of Sst2. In strains that are defective in RGS activity, there is a shift in localization in the exocytic protein, Exo84 (Kelley et al. 2015). Furthermore, it has been shown that Bni1 is involved in endocytic pathways (Prosser et al. 2011).

Yeast, much like other eukaryotes, undergo clathrin mediated endocytosis (CME). CME is induced through a three-step process in which clathrin binds a target area, actin is assembled around clathrin in an Arp2/3 dependent manner forming an invagination, which is cleaved by scission proteins (Kaksonen and Roux 2018; Goode, Eskin, and Wendland 2015). Recently it has been shown that yeast possess clathrin independent endocytic routes, dependent on the formin Bni1 activated by Rho1 (Prosser et al. 2011). Additionally, the Kelch proteins, Kel1 and Kel2, are able to bind the endocytic proteins, End3 and Pan1, respectively(Whitworth et al. 2014). In mammalian cells it has been found that the timescales of CME and CIE are much different form one another, in which CME occurs on the scale of tens of seconds, while CIE may be as quick as hundreds of milliseconds (Goode, Eskin, and Wendland 2015). This difference in timescales may reflect the specific processes affected by either class of endocytosis. The use of CIE may be important for the yeast pheromone response in order to accurately track a pheromone source.

We hypothesized that MAPK phosphorylation of the RGS would influence its spatiotemporal activity during the pheromone response. Here we demonstrate that Gα bound MAPK regulates RGS localization, which in turn alters the localization of Gα-MAPK. We determined that the post-translational modification of the RGS inhibits endocytosis through the formin regulating protein Kel1. Furthermore, we provide evidence that the formin Bni1 is preferentially used during the pheromone response and that the changes in endocytosis are likely happening specifically in Clathrin independent endocytosis. These results lead us to conclude that endocytosis during the pheromone response is a dynamic process that is controlled through a Gα-MAPK feedback loop to the RGS.

CHAPTER 2

METHODS

2.1 Plasmid Construction

The pRSII405-SST2-GFP plasmid listed in Table1 was generated by amplifying genomic SST2-GFP from strain SST2-GFP-c9 listed in Table 2 using primers WSM 28 and WSM 29 found in Table 3. pRSII405 and SST2-GFP were digested with restriction enzymes BamHI and KpnI (New England Biolabs) as previously described (Dixit et al. 2014). The pRSII405-*sst2*^{S539A}-GFP plasmid listed in Table 1 was generated from pRSII405-SST2-GFP by PCR site-directed mutagenesis (New England Biolabs) using oligonucleotides WSM 37 and WSM 38. Sequencing verification of pRSII405-*sst2*^{S539A}-GFP was performed using primer WSM 25. Plasmids were integrated into yeast strains using BlpI (New England Biolabs).

pMAL-c5X-SST2-GFP, pMAL-c5X-TEV-*sst2*^{S539A}-GFP, and pMAL-c5X-TEV-*sst2*^{S539D}-GFP plasmids were generated by amplifying genomic regions with primers JKM 28 and JKM 30, digesting with NotI-HF and EcoRI-HF (New England Biolabs), and ligating into pMAL c5X (gift of Dorothy Croall) using T4 DNA Ligase (New England Biolabs). Verification of insertion was performed through restriction digest using EcoRI-HF and NotI-HF. pMAL-c5X KEL1 was generating by amplifying genomic KEL1 using primers JKM 31 and JKM 35. PCR product and vector were digested using Not1-HF and SalI-HF.

Digests were carried out at 37°C for 2 hours, with addition of 1uL of calf intestinal alkaline phosphatase (New England Biolabs) to the digested vector for the final 10 minutes to dephosphorylate the 5’ end. Ligation of digested vector and insert were carried out with a 3:1

ratio performed at room temperature for 10 minutes and heat inactivated at 65°C for 10 minutes. The ligation reaction was allowed to cool on ice, then transformed into competent DH5a E. coli using standard heat shock techniques.

2.2 Yeast Strains

Yeast strains used in this study are shown in Table 2. Strains were constructed in the MATa haploid Saccharomyces cerevisiae strain, BY4741. Proteins were tagged with GFP or Ruby at its chromosomal locus through oligonucleotide-directed homologous recombination with GFP-spHIS5 amplified with primers listed in Table 3 from the tagging vectors listed in Table 1 (Lee, Lim, and Thorn 2013) or the GFP collection(Huh et al. 2003). Sst2 phosphomutants were made by integrating the codon of interest with a PCR amplified CORE cassette(Storici and Resnick 2006). Deletions were performed by first amplifying the genomic locus from the Mata haploid deletion collection (Dharmacon) with primers listed in Table 3 and transformed using the standard high efficiency lithium acetate transformation.

Cells were grown in rich medium (YPD) or synthetic medium (SC) at 30°C unless otherwise indicated. PCR products were transformed into yeast strains using standard lithium acetate transformation procedure. Individual colonies were isolated by growth on standard selective media (SC leu-, SC ura-, SC his-,), selective media with 5-fluoroorotic acid, or YPD selective median (YPD G418+). Transformants were verified using fluorescence microscopy, sequencing, and/or PCR.

2.3 Yeast Agarose Pad Imaging

Yeast were imaged on an Olympus IX83 with a 60X-TIRF 1.49 NA objective, a Photometrics Prime95b camera, Xcite LED 120 Boost fluorescence light source (Excelitas), and filters for DAPI and GFP (Semrock). Cells were grown to mid-log phase (OD600 = 0.1 to 0.8) at 30°C in Synthetic Complete Media with 2% dextrose (SCD) and then imaged on pads made of 2% agarose in SCD. Imaging was performed with an objective heater (Bioptechs) set to 30°C. Cells were pelleted and then resuspended in SC with 3uM α-factor and placed on an agarose pad as above. Images were deconvolved using Huygens (SVI) with the CMLE. Images were quantified using FIJI (Schindelin et al. 2012) and MATLAB (Mathworks).

2.4 Microfluidics Experiments

Microfluidic devices were made by using a Silicone polymer poured onto a microfluidics device mold (gift of Scott Collins and Rosemary Smith). SYLGARD 184 Silicone Polymer was mixed at a ratio of 10:1, part A to part B, using a glass stirring rod to mix (Dow). Mixed polymer was poured onto the device mold and placed in a vacuum chamber for 1hr. After all air bubbles were removed, the mixture was placed in an oven at 80°C for 1hr. After cooling to room temperature, devices were cut out using a razor and ports were punctured using an 18g Leuer stub. Prepped devices and coverslips were cleaned by spraying with methanol, ethanol, then water, and dried using an air hose. Devices and coverslips were then placed in a Harrick Plasma PDC32G Cleaner for 45s. to remove remaining organic matter and allow the fusion of the device to the cover slip.

Cultures were grown in SC to an OD600 between 0.1–0.8 at 30°C. Live-cell microfluidics experiments were performed using an IX83 (Olympus, Waltham MA) microscope with a Prime 95B CMOS Camera (Photometrics). Fluorescence and Differential Interference Contrast (DIC) images were acquired using an Olympus-APON-60X-TIRF objective. Z-stacks of GFP and RFP images were acquired using an Xcite 120 LEDBoost (Excelitas). Cells were imaged in a microfluidic device based on the Dial-a-wave design that allows for the rapid switching of media while holding the yeast in place (Figure A1) (Bennett 2008, Dixit 2014). Pheromone addition was verified using AlexaFluor 647 dye (Life Technologies) imaged with 1 Z-slice. Cells were imaged at 20 min intervals for 12 hours for 300nM experiments and 5 min intervals for 0-150nM experiments. Images were deconvolved using Huygens Software (Scientific Volume Imaging, Hilversum, Netherlands) Classic Maximum Likelihood Estimation (CMLE) Deconvolution Algorithm. Masks of cells were made using ImageJ (Schindelin et al. 2012) and data analysis was performed using MATLAB (MathWorks, Natick, MA). Experiments probing endocytosis omitted AlexaFluor 647 dye and relied on diffusion of SynaptoRed (Millipore)(Vida and Emr 1995). SynaptoRed was used at a concentration of 0.6uM in all microfluidic experiments.

2.5 Image Analysis

To quantify the fraction of protein localization over time, MATLAB was utilized. Masks of cells were loaded into MATLAB and each cell was labeled over time to track individual cells over time. The fluorescent intensity of each fluorescent protein was extracted over time using a line width of 5 pixels as previously described (Kelley et al. 2015). Peak Bem1 was used as a reference to normalize the distribution of proteins of interest in relation to the polar cap. This

was done by setting peak Bem1 as the midpoint and shifting the protein of interest in the same manner. A diagram of this analysis is shown in Figure 1B. The normalized fluorescence intensity was plotted at each point along the cell periphery with shaded regions showing 95% confidence intervals. Statistical analysis was performed between profiles using a one-way ANOVA and Tukeys honest significance test (HSD) with p values <0.05 denoted as significant.

To quantify endocytic rates over time, masks were made using FIJI to define each cell. A second mask was made to define the internal area of the cell, by eroding the original mask 3-4 times, ensuring the periphery was excluded. Using MATLAB, a third mask was defined for the periphery by subtracting the original mask from the internal mask (Figure C1). The fluorescent intensity of the maximum project images at each pixel was captured and the mean intensity was found at each timepoint on an individual cell basis. This was done on all three masks to define the mean whole, peripheral, and internal fluorescence. The ratio of internal to external accumulation was calculated to normalize for delayed SynaptoRed diffusion into the microfluidics chamber, as cells internalization rate of SynaptoRed is dependent on the peripheral accumulation. Bar graphs of the means of internal to external fluorescence ratios are plotted with error bars denoting the standard error of the mean (SEM).

CHAPTER 3

RESULTS

3.1 RGS Localization is Highly Dynamic

The main RGS in yeast, Sst2, is known to be necessary to allow proper desensitization from signaling through the GPCR, Ste2 (Dohlman et al. 1996). Studies have confirmed that Sst2 is upregulated upon exposure to pheromone, and that disruption of RGS activity, through deletion or mutation, causes a 10-100 fold increase in pheromone sensitivity (Apanovitch et al. 1998; Ballon et al. 2006; Dixit et al. 2014). Additionally, it has been shown that Sst2 is regulated by the MAPK during the pheromone response, so we sought to understand how Sst2 localizes during the pheromone response, and how these localizations affect G-Protein Signaling. We hypothesized that the localization of Sst2 would change over time, based on the need to spatially shut down signaling. To understand the dynamics of RGS, we transformed cells to endogenously express a C-terminal GFP tagged SST2. With this fluorescently tagged strain, we observed the localization of Sst2-GFP over a two-hour period on agarose pads. Otherwise WT strains expressing Sst2-GFP were exposed to 3μM pheromone at 30°C for the specified intervals at 0 min., 30 min., 60 min., and 90 min before being imaged. Cultures were concentrated through centrifugation and resuspended in Synthetic Complete Media (SC) containing pheromone. The localization of Sst2-GFP is highly dynamic, with changes in localization being dependent on when Sst2 is observed (Figure 1C). During mitosis, Sst2 is mostly homogeneously

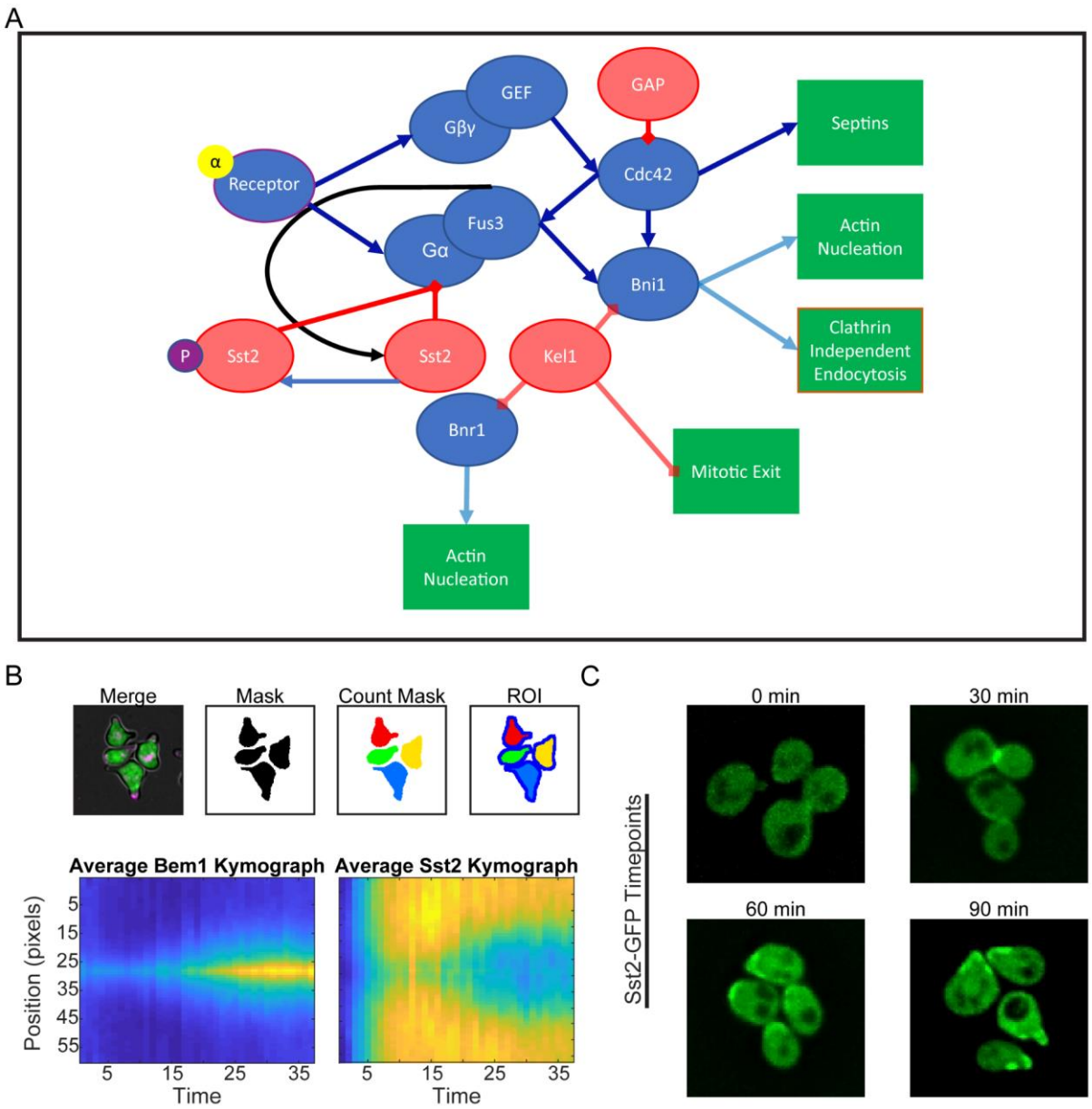

Figure 1. Yeast Mating Pheromone Pathway and Dynamics of the RGS.

A) Diagram of the mechanism in the yeast pheromone pathway displaying known interactions and outputs of downstream effectors. B) Workflow of methods in quantitative image analysis. Representative masks are shown and the corresponding kymographs of an example localization of Bem1 and Sst2 over time. C) Representative pseudo color images of the dynamics of Sst2-GFP localization at single timepoints ranging from 0 min to 90 min.

distributed through the cell, though in early time points of pheromone exposure, Sst2 can be seen localizing to the bud neck. This early localization of Sst2 is thought to be occurring before

or during mitotic exit. As the pheromone response progresses, Sst2 can be seen localizing at the polar cap and at septin structures. From these experiments we were able to conclude that the localization of the RGS is highly dynamic and dependent on timing in the pheromone response.

3.2 RGS Activity Allows Septin and Polar Cap Separation

With the observation that Sst2 localization is highly dynamic, we next sought to determine if the localization of Sst2 is dependent on its established binding partners: the GPCR, Ste2, and the Gα subunit, Gpa1. Sst2 is targeted to active signaling through its DEP domain, promoting association with the receptor to perform its GAP activity on Gα through the RGS Sst2 domain (Ballon et al. 2006). In addition to this localization Sst2 has been observed in the area of septins (Kelley et al. 2014). In this study the authors concluded that the RGS promotes gradient tracking through proper septin deposition. Septins are proteins deposited to act as barriers, allowing separation of the mother and daughter cells during mitosis, and is proposed to act as a biochemical barrier during the pheromone response(Takizawa et al. 2000; Kelley et al. 2015). As yeast progress through the pheromone response, the polar cap grows out from the center of the cell and septins are deposited at the base of the shmoo (Giot and Konopka 1997; Longtine, Fares, and Pringle 1998). Through the pheromone response the separation between the polar cap and septins becomes greater and it is thought that the septins are necessary to contain the polar cap in one region, allowing proper growth (Kelley et al. 2015). The previous study utilized a strain that inhibited the ability of Sst2 to accelerate GTP hydrolysis on the Gα subunit, $gpa1^{G302S}$, known as the UnGAPable Gα mutant, causing an inability to separate septins from the polar cap and leading to a defect in the ability to track the pheromone gradient (DiBello et al. 1998; Kelley et al. 2015). We have shown that Sst2-GFP associates in the region of

septins at individual time points and therefore hypothesized that Sst2 has more interactions that receptor and the Gα subunit. To test this hypothesis, we examined localization of Sst2-GFP in a *gpa1*^{G302S} mutant and predicted to see a collapse in the polar cap and Sst2 separation, much like that seen with septins previously (Kelley et al. 2015).

To track individual cells throughout their whole response, we used a custom microfluidics device that allows the delivery of fresh media for the duration of the experiment and pheromone in either a constant concentration, or in a gradient to examine tracking. We observed the localization of Sst2-GFP relative to the polar cap in the WT and *gpa1*^{G302S} background strains. We examined Sst2-GFP in a dual tagged strain with Bem1-Ruby expressed under the endogenous promoter in both the WT and *gpa1*^{G302S} background. Bem1 was tagged as it acts as a scaffold to Cdc42-GTP, serving as a readout for active Cdc42 and as a reference point to the polar cap for our protein of interest (Gulli et al. 2000; Ogura et al. 2009). A representative diagram of this analysis is shown in Figure 1B. Microfluidics experiments were performed with cells exposed to saturating pheromone (300nM) and imaged at 20 min intervals for 12hrs. To quantify the localization of Sst2-GFP over time, we measured the fluorescence intensity at points along the periphery of the cell. To normalize the localization of Sst2-GFP to the polar cap, we utilized the profile of maximum Bem1-Ruby. The peak of Bem1-Ruby's localization was set as the midpoint of the graph and the profile of Sst2-GFP protein was aligned in the same manner. To quantify only pheromone responsive time points for all cells, data were quantified starting at the 160 min. time point. The normalized fluorescence intensity of each protein was plotted against position along the cell. Thousands of profiles across dozens of cells were averaged to understand the dynamics of Sst2-GFP over time.

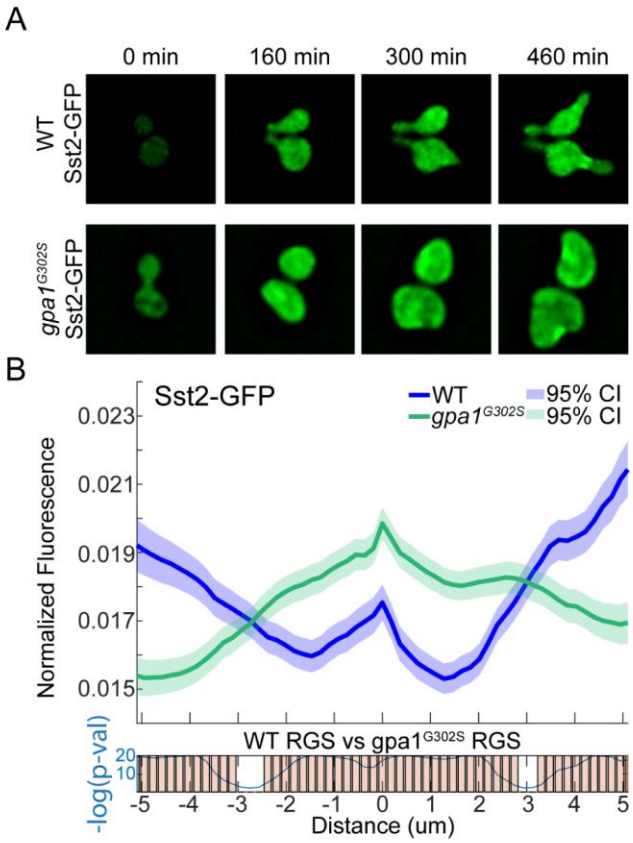

Figure 2. RGS Localization is Dependent on its' GTPase Activity.

A) Representative images of WT and *gpa1*^{G302S} Sst2-GFP over the course of a microfluidics experiment. Disruption of Sst2 function results in a collapse in the polar cap septin separation. B) Quantification of the spatial distribution of Sst2-GFP normalized to peak Bem1-Ruby (not shown) in both WT and *gpa1*^{G302S} mutant. Bottom graphs display statistical analysis using one-way ANOVA followed by Tukey's HSD, with statistically (<0.05) significant differences in localization noted by bars. Data is derived from n = 2848 (WT) and n = 3132 (*gpa1*^{G302S}) data points per position along the periphery.

We found that the localization of Sst2 is dependent on its ability to inactivate the Gα subunit (Figure 2A). In WT cells, Sst2 localizes to both the septin areas and the shmoo tip, though when RGS activity is abrogated, septin structures overlap with the polar cap and become less separated as the experiment progresses. In WT cells, the maximum Sst2-GFP intensity is peripheral to the polar cap, although some still colocalizes with the polar cap (Figure 2B). In the *gpa1*^{G302S} mutant, a larger proportion of the Sst2-GFP colocalizes with the polar cap

(Figure 2B). These changes in Sst2 localization are consistent with the changes seen in septin localization in these strains and suggests that the localization of Sst2 is dictated by proper septin deposition (Kelley et al. 2015).

3.3 RGS Localizes Differentially from Receptor

To further understand the dynamics of the localization of Sst2, we observed the localization of the GPCR Ste2 to compare the localizations and determine if Sst2 association with septins is due to receptor being associated there as well. Having determined that the ability of Sst2 to interact with Gα and promote the hydrolysis of bound GTP is necessary for its proper localization, we wanted to test whether the localization of Sst2 was coincident with that of the receptor, Ste2. Previous studies have shown that Sst2 is needed in order to allow proper receptor localization to the polar cap (Venkatapurapu et al. 2015), suggesting that the localization of these proteins must be coincident if Sst2 did not possess other interactions. We hypothesized that Sst2 may possess different binding partners other than the receptor and Gα, due to fact that Sst2 follows septin localization patterns, where signaling is not thought to be actively occurring. To test this hypothesis, we examined the spatiotemporal dynamics of Ste2 and Sst2 in cells responding to pheromone (300nM). Attempts were made to produce a dual tagged fluorescent strain with Sst2 and Ste2, though a GFP tag was the only tag tested that would provide WT localizations with each of these proteins. To overcome this hurdle, we utilized our reference protein, Bem1-Ruby, in both WT Sst2-GFP and Ste2-GFP strains.

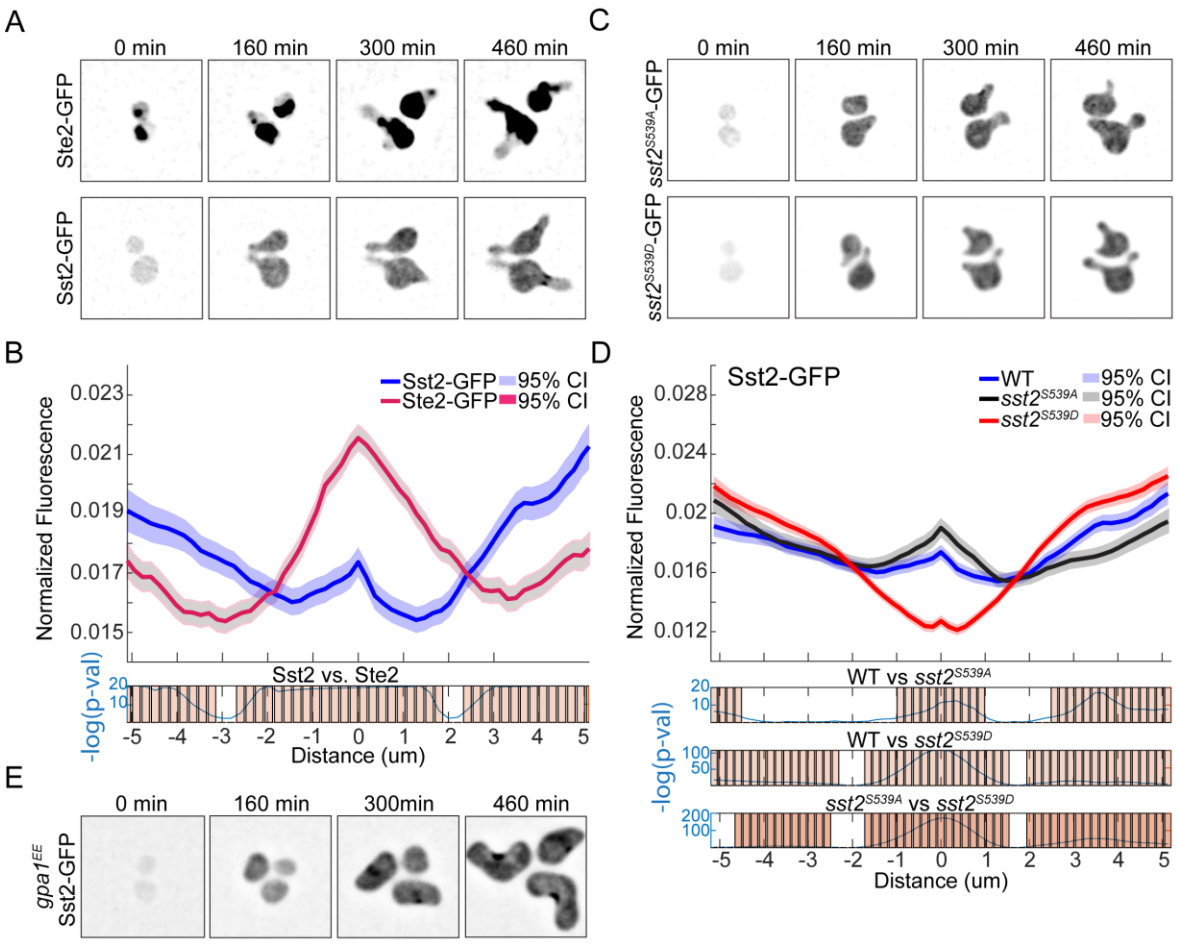

Figure 3. RGS Localizes Differentially from Receptor and is Dependent on Phosphorylation by Gα bound MAPK.

A) Representative images of WT Sst2-GFP and Ste2-GFP over the course of a microfluidics experiment. B) Quantification of the spatial distribution of Sst2-GFP and Ste2-GFP with statistical analysis below showing statistically significant associations noted by bars. Data are derived from two independent experiments with n = 2848 (Sst2-GFP) and n = 3328 (Ste2-GFP) data points per position. C) Representative images of the Sst2-GFP phosphomutants, *sst2*^{S539A} and *sst2*^{S539D} over a 12hr microfluidics experiment. D) Quantification of the localization of Sst2-GFP in the WT and phosphomutants with statistical analysis below. Data are derived from two independent experiments with n = 2816 (*sst2*^{S539A}) and n = 4448 (*sst2*^{S539D}) data points per position. E) Representative images of *gpa1*^{EE} Sst2-GFP over a microfluidics experiment. The localization of Sst2-GFP appears to be that near WT association.

Microfluidics experiments were performed with each strain and the localization of each protein was quantified relative to Bem1 from data derived from two independent experiments.

Analysis of representative images of cells at different time points (Figure 3A) shows that throughout the time course experiment, Ste2-GFP associates to regions of the polar cap as well as the vacuole, as previously observed (Venkatapurapu et al. 2015; Jenness and Spatrick 1986). The vacuolar association is mainly due to degradation of active receptor, causing accumulation of the stable GFP tag in the lysosomal compartments. The non-vacuolar association of the receptor is seen at the growing shmoo and just behind the growing shmoo. As our interests lie only in receptor that may be signaling or present on the membrane, as opposed to being associated with the vacuole, we only quantified peripheral Ste2-GFP. To ensure we were not quantifying vacuolar Ste2-GFP, a script was written to remove vacuolar fluorescence (Figure 1B). Masks were made of the vacuole and the fluorescence of the area was set equal to the extracellular background fluorescence. Quantification of the localizations of each of these proteins normalized to peak Bem1 reveals a difference in their localizations (Figure 3B). The receptor has strong association with the polar cap, while Sst2 has associations with both the polar cap and peripheral regions, thought to be septins. This difference in localization lead us to propose the localization of Sst2 is dependent not only on the receptor and Gα, but also through currently unknown binding partners.

3.4 Phosphorylation of the RGS Controls Its Localization

Sst2 is phosphorylated by the pheromone responsive MAPK, Fus3, at serine 539, though the effect of this regulation is not well understood (Garrison et al. 1999). Previous studies have shown that the phosphorylation state of Sst2 does not affect the yeast's mating ability, output through Gβγ pathways, nor sensitivity to pheromone (Garrison et al. 1999). It had been reported that phosphorylation of Sst2 may stabilize the protein, though the mechanism of this

preservation is unknown. Additionally, these parent studies examining the regulation of Sst2 sought to use only standard biochemical approaches. As localization of proteins influences their function, we proposed using live cell fluorescence microscopy as a new approach to this decade old question. We hypothesized that the phosphorylation of Sst2 must control its ability to localize, as the previous studies found no differences in signaling through the pheromone pathway.

We developed C-terminal tagged Sst2-GFP point mutants, the unphosphorylatable *sst2*^{S539A}, and the phosphomimetic *sst2*^{S539D}. Using the same imaging conditions as the otherwise WT Sst2-GFP strain, we tracked the spatiotemporal localization of both phospho-mutants over a 12hr period. The phosphorylation state of Sst2 influences its spatiotemporal localization (Figure 3C). The phosphomimetic mutants have abrogated septin association, though Sst2 is still able to associate with the polar cap. In its unphosphorylated state, Sst2 appears to have near WT association with the septins and polar cap, although to a lesser degree. Quantification of the localization of the phosphomutants over the 12hr period reveals a significant difference in the localization between the WT vs. phosphomimetic strain and the unphosphorylatable vs. phosphomimetic strain. The WT vs. unphosphorylatable strain had some significant differences, particularly in the polar cap region, though these two strains had the most appreciable similarities in localization. Qualitatively there is septin association in these two strains, while the septin association is lacking in the unphosphorylatable strain. These data allow us to conclude that the localization of Sst2 is dependent on its phosphorylation state.

To fully understand the dynamics of Sst2 phosphorylation, we turned our attention toward the MAPK, Fus3, which is responsible for the phosphorylation event (Garrison et al.

1999). It has been well characterized that the MAPK localizes to the nucleus, cytoplasm, and cell periphery throughout the pheromone response. In the nucleus it is responsible for controlling transcriptional output through phosphorylation of the transcriptional inhibitors, Dig1/2 and the transcription activator, Ste12 (Maeder et al. 2007; Chen et al. 2010; Tedford et al. 1997; Roberts et al. 2000; Hung et al. 1997). In the cytoplasm, MAPK is known to interact with both the scaffolding protein Ste5 and the Gα subunit (Metodiev et al. 2002; Elion 2001). As there has been no observation that Sst2 localizes to the nucleus, we did not expect this is where phosphorylation of Sst2 was occurring. MAPK association with Ste5 has been found to be necessary to activate the MAP through the MAPK signaling cascade, though it is not thought that Ste5 bound MAPK is responsible for phosphorylating substrates at the cell periphery during the pheromone response (Elion 2001). We therefore hypothesized that Gα bound MAPK is responsible for phosphorylating Sst2. If this association is responsible for the phosphorylation event, we expected a phenotype most similar to that of the unphosphorylatable mutant, as well as an association of Sst2 most similar to this mutant or the WT.

To understand this interaction, we utilized a double point mutant in which the Gα subunit is no longer able to bind the MAPK, $gpa1^{R21ER22E}$, known as $gpa1^{EE}$ (Metodiev et al. 2002; Errede et al. 2015). Upon mutating this site, the strain was observed in a microfluidics device with saturating pheromone (300nM) and imaged every 20 min for 12 hrs. We found that abrogating the MAPK-Gα interaction has qualitatively little effect on the localization of Sst2 (Figure 3E). Further analysis of the localization using standard computational methods will be necessary to determine if there is a quantitative difference between this mutant and the WT strain. Sst2-GFP is still able to interact with both the septins and the polar cap over time,

localizing in much the same way as WT cells, apart from the morphological changes induced by the *gpa1*^{EE} mutation (Figure 3E). As the localization of the unphosphorylatable Sst2 is very similar to that of WT Sst2-GFP, it is difficult to conclude that Gα bound MAPK is responsible for the phosphorylation of Sst2, but the result is consistent with that hypothesis. To further understand the dynamics underlying Sst2 phosphorylation and what this might mean for the pheromone response, we sought to address whether there was feedback to the MAPK, influencing its' localization and activity.

3.5 MAPK Localization at the Polar Cap is Driven by Gα

Fus3 is the final MAPK in the MAPK signaling cascade and is responsible for phosphorylating multiple substrates, both in the nucleus and in the cytoplasm. Two of the main cytosolic binding partners of the MAPK are the heterotrimeric Gα subunit, thought to be responsible for binding MAPK and allowing directed substrate phosphorylation, as well as the scaffold protein, Ste5, recruiting the MAPK signaling cascade components to sites of active Gβγ (Elion 2001; Errede et al. 2015). We hypothesized that the localization of the MAPK at the polar cap is largely dependent on the Gα interaction. To test this hypothesis, we produced strains with C-terminally tagged Fus3-GFP as well as Bem1-Ruby in a WT and *gpa1*^{EE} background. These strains were observed in a microfluidics device exposed to 300nM pheromone and imaged every 20 min. for 12 hrs. Disruption of the interaction between the Gα subunit and MAPK prevents the proper localization of MAPK to the polarity patch (Figure 4A & 4E).

Quantification of the time course reveals a broadened distribution of the MAPK along the periphery of the polar cap in the *gpa1*^{EE} strain compared to that of WT cells (Figure 4B). The

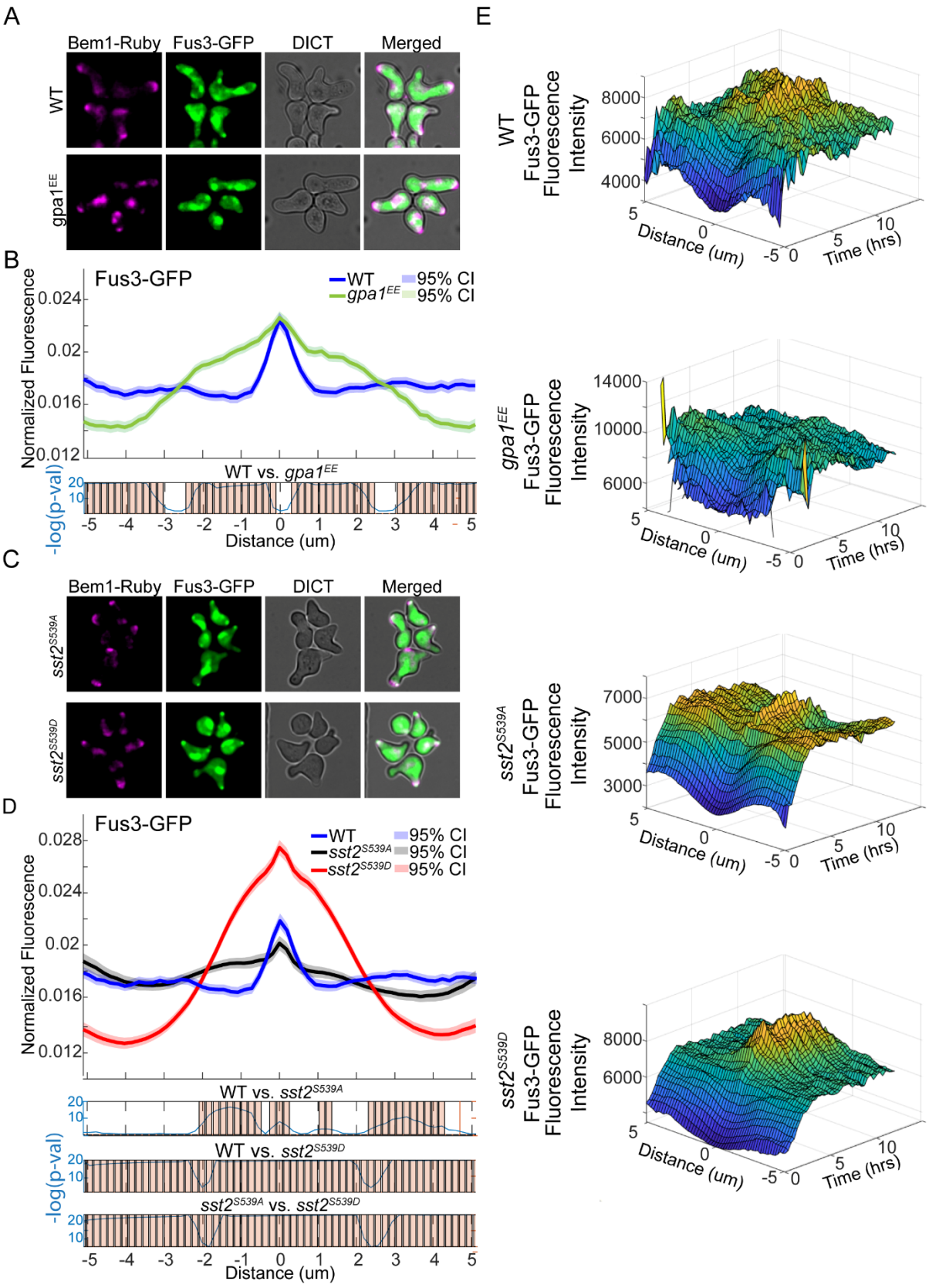
A
Bem1-Ruby
Fus3-GFP
DICT
Merged
WT
gpa1EE
B
Fus3-GFP
WT
95% CI
gpa1EE
95% CI
Normalized Fluorescence
0.024
0.02
0.016
0.012
WT vs. gpa1EE
-log(p-val)
20
10
-5 -4 -3 -2 -1 0 1 2 3 4 5
Distance (um)
C
Bem1-Ruby
Fus3-GFP
DICT
Merged
sst2S539A
sst2S539D
D
Fus3-GFP
WT
95% CI
sst2S539A
95% CI
sst2S539D
95% CI
Normalized Fluorescence
0.028
0.024
0.02
0.016
0.012
WT vs. sst2S539A
WT vs. sst2S539D
sst2S539A vs. sst2S539D
-log(p-val)
20
10
-5 -4 -3 -2 -1 0 1 2 3 4 5
Distance (um)
E
WT Fus3-GFP Fluorescence Intensity
8000
6000
4000
5 0 -5
Distance (um)
0 5 10
Time (hrs)
gpa1EE Fus3-GFP Fluorescence Intensity
14000
10000
6000
5 0 -5
Distance (um)
0 5 10
Time (hrs)
sst2S539A Fus3-GFP Fluorescence Intensity
7000
5000
3000
5 0 -5
Distance (um)
0 5 10
Time (hrs)
sst2S539D Fus3-GFP Fluorescence Intensity
8000
6000
5 0 -5
Distance (um)
0 5 10
Time (hrs)

Figure 4. MAPK Localization Determined by Gα and the Phosphorylation State of the RGS.

A) Representative images of WT and *gpa1*^{EE} Fus3-GFP Bem1-Ruby. B) Quantification of the spatial distribution of Fus3-GFP with statistical analysis below showing statistically significant associations noted by bars. Data are derived from two independent experiment with n = 2848 (WT) and n = 3328 (*gpa1*^{EE}) data points per position. C) Representative images of Fus3-GFP in Sst2 phosphomutants. D) Quantification of the localization of Fus3-GFP in the WT and phosphomutants with statistical analysis below. Data are derived from n = 4031 (*sst2*^{S539A}) and n = 3741 (*sst2*^{S539D}). E) 3-D kymographs of Fus3-GFP in each strain.

less focused distribution of the MAPK is consistent with the MAPK being removed from the polar cap. Residual association aligned with the polar cap is consistent with MAPK associating with the scaffolding protein, Ste5, which brings MAPK into close proximity to the other MAPK's involved in the signaling cascade (Elion 2001). Additionally, quantifying the average amount of MAPK through the 12hr time course shows a decrease the amount of MAPK found on the periphery of the membrane in the *gpa1*^{EE} strain compared to that of WT (data not shown). Disruption of the MAPK localization through mutation of the Gα subunit and the finding that lower levels of MAPK localize in the docking mutant shows that the Gα subunit is responsible for targeting the MAPK to sites of active signaling to phosphorylate multiple substrates.

3.6 Phosphorylation State of RGS Influences MAPK Localization

Since the localization of Sst2 is dependent on phosphorylation by MAPK, we sought to determine if there was a feedback mechanism in which the localization of Gα bound MAPK was affected as well. Fus3-GFP was tagged in both the WT, unphosphorylatable, and phosphomimetic Sst2 strains. As before, Bem1-Ruby was used as a reference marker. Observing the localization of MAPK in these three strains show that the phosphorylation state of Sst2 affects the localization of Fus3 (Figure 4C). Although the localization of MAPK in these two mutants appears to be very similar when observing just MAPK-GFP, when the profiles are

adjusted relative to active Cdc42 (Bem1-Ruby), a surprising difference is seen in which the phosphomimetic mutants has a stronger localization at the polarity patch (Figure 4D & 4E). Notably the distribution of MAPK in the phosphomimetic strain appears broader with a larger amplitude compared to the otherwise WT strain. To account for this difference in localization, we considered whether the phosphorylation of Sst2 prevents MAPK from being removed through recycling pathways. It is well documented that during the pheromone response, cells need to both deliver new membrane and pheromone responsive proteins to the membrane through exocytosis (Dyer et al. 2014) and need to recycle proteins and materials through endocytosis. In order for these vesicle trafficking processes to occur, a myriad of proteins need to be present at sites of active signaling. These proteins, such as the formins, Bni1 and Bnr1, are necessary to set up actin, while others are needed for proper regulation, such as the Kelch protein Kel1 (Karpova et al. 1998; Gould et al. 2014). In yeast two hybrid assays, it has been found that Sst2 interacts with Kel1 and Bnr1, though the outcome of these potential interactions is not well understood (Burchett et al. 2002). For this reason and the fact that Sst2 localizes to the bud site, much like Bni1, Kel1, and Bnr1, we sought to better understand the spatiotemporal dynamics of Sst2 over time in a variety of deletion mutants, seeking to uncover novel interactions of Sst2 separate from the receptor and Ga.

3.7 RGS Localization is Dependent on Formins and Kelch Proteins

While studying the spatiotemporal localization of Sst2, we noted an early association of Sst2-GFP to areas of the bud neck at early time points in the pheromone response (Figure 1C). The association of Sst2 was observed between 20-60min., before the mother and daughter cells had finished mitosis and before shmoo formation had started to occur, with only one other

reported observation of this occurring (Dixit et al. 2014). Due to this observation and a yeast two hybrid showing Sst2 interacts with Kel1 and Bnr1, we wanted to determine if there were in vivo binding interactions to allow proper pheromone signaling and examine if these may be related to observed changes in MAPK. We hypothesized that Sst2 and Kel1 would interact with

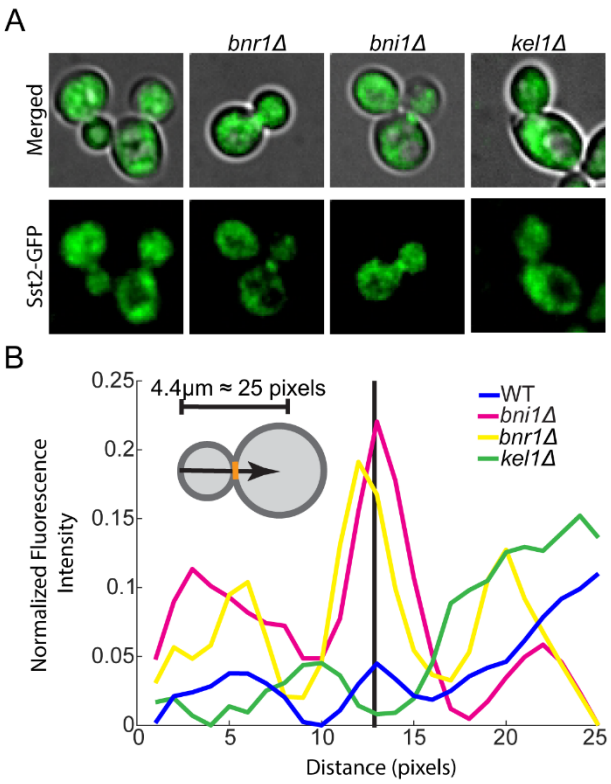

Figure 5. RGS Mitotic Localization is Enabled by Kel1.

A) Representative images of Sst2-GFP in deletion mutants *bnr1Δ*, *bni1Δ*, and *kel1Δ* at early time points during microfluidics experiments. B) Representative quantification of the spatial distribution of Sst2-GFP through the mother and daughter cell from the images shown in A. The top right diagram shows the analysis performed to measure Sst2-GFP fluorescence, measuring from the daughter cell to the mother cell with the midpoint located at the bud neck corresponding to the central black line.

one another, to form an axis of control of the formins.

To understand how the spatiotemporal localization of Sst2 over time is affected by the formins and kelch proteins, we integrated a C-terminal GFP tag to be endogenously expressed

in cells lacking either Bni1, Bnr1, or Kel1. Microfluidic experiments were performed in each one of these deletion strains and the localization of Sst2 was quantified compared to peak Bem1 over the 12hr time course experiments. Representative images show Sst2s localization during the early time points of the microfluidics experiments (Figure 5A). As shown in this figure, deletion of Kel1 removed Sst2-GFP from the bud neck. Due to the fact that Sst2 does not localize to the bud neck in every cell, we examined all recorded images to attempt to find localization. In the WT, *bni1Δ*, and *bnr1Δ* strains we were able to find a number of cells with this localization. In the *kel1Δ*, the image shown was thought to have the most amount of bud neck localization. Qualitatively it may be difficult to say whether there is appreciable localization at the bud neck or not, therefore we measured the fluorescence intensity profiles (Figure 5B) for each of the images (Figure 5A). Equal length line profiles were drawn beginning in the daughter cell and ending in the mother cell. The center of the line placed directly at the bud neck, as is noted by the vertical black line (Figure 5B). A representative diagram of this analysis is displayed in the top left corner of Figure 5B. Through both qualitative and quantitative analysis, it is shown that association of Sst2 to the bud neck is seen in all deletion mutants, except when *KEL1* is deleted, leading us to conclude the association of RGS with the bud neck during mitosis is Kel1 dependent. Conversely, deletion of the formin Bni1 or Bnr1 shows a quantitatively larger amount of RGS associated with the bud neck at this time, leading us to conclude removal of Sst2 may be formin dependent.

The largest changes in both morphology and the localization of Sst2 is seen in deletions of *BNI1* and *KEL1*, which appear to have opposing effects. Deletion of the formin Bnr1 has little effect on the pheromone response, as these cells form near WT shmoos, with the ability to

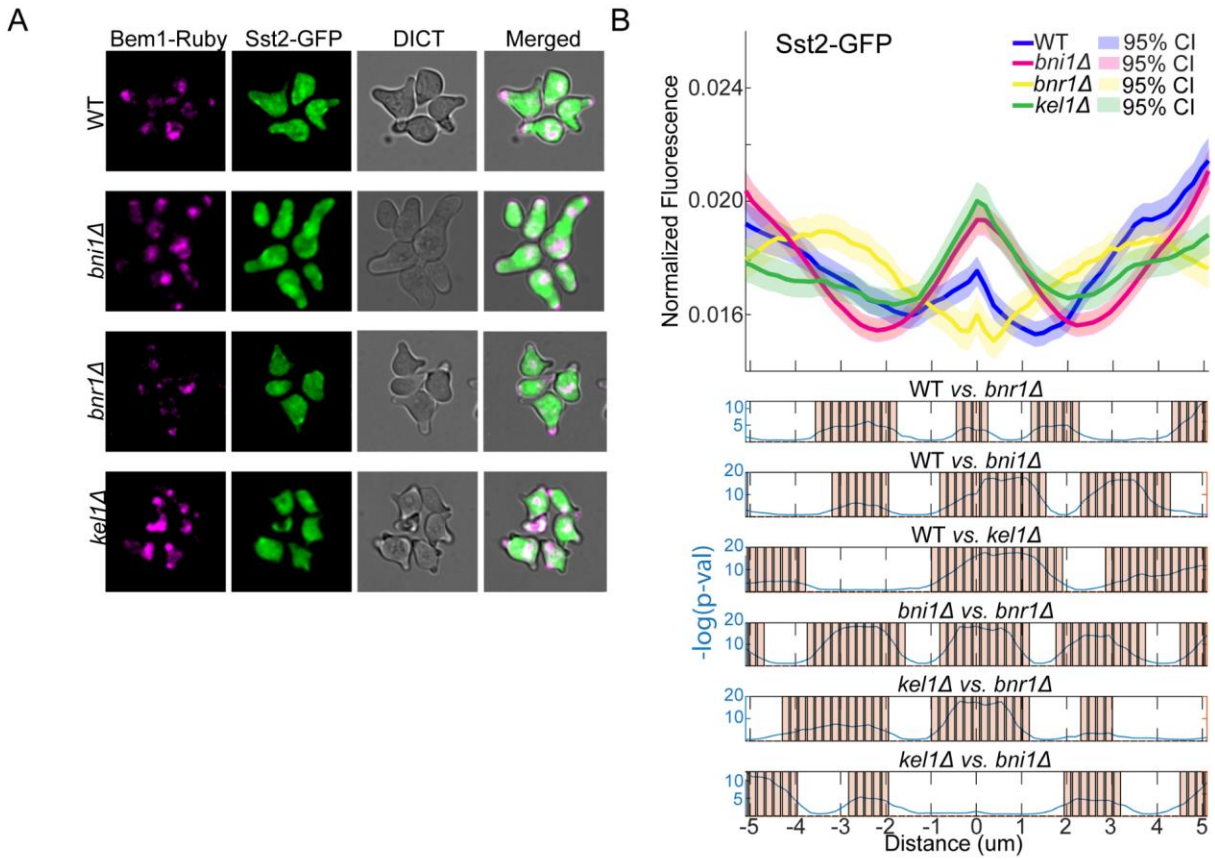

Figure 6. RGS Localization is Affected by the Formin Bni1 and Kelch Protein Kel1.

A) Representative images of Sst2-GFP in WT, *bnr1Δ*, *bni1Δ*, and *kel1Δ* at time 8hrs in a microfluidics experiment. The morphology of cells is greatly affected in *bni1Δ* and *kel1Δ* mutants. B) Quantification of the localization of Sst2-GFP in the WT and deletion mutants with statistical analysis below. Data are derived from two independent experiments with n = 2581 (WT), n = 4176 (*bni1Δ*), n = 1189 (*bnr1Δ*), and n = 3161 (*kel1Δ*) data points per position.

form between 2 to 3 shmoos over a 12hr period (Figure 6A). Deletion of *BNI1* results in cells that have much longer, broader shmoos, and the cells seem to form just one or two shmoos total during the 12hr. response. On the other hand, deletion of *KEL1* results in the cells forming short, tight shmoos, with the ability to form up to six shmoos during the duration of the response. Looking at the localization of Sst2 in these three mutants, we find the localization of Sst2 is influenced by deletion of *BNI1* or *KEL1* (Figure 6B). Deletion of the formin *BNR1*, results

in a distribution of Sst2 most similar to WT, though there are areas of statistically significant difference compared to that of the WT localization. The localization of Sst2 in both the *bni1Δ* and *kel1Δ* quantitatively appear very similar to one another. The stronger association of Sst2 in regions of the polar cap is seen most strongly qualitatively upon deletion of *BNI1* (Figure 6A). The association of Sst2 at the polar cap in *kel1Δ* cells may be due to the small shmoo structures, in which the septins are in close proximity to the polar cap and may therefore be measured in regions of the polar cap. These data suggest the formin, Bni1, and kelch protein, Kel1, may have less defined functions during the pheromone response in terms of their interactions with Sst2. The most significant change in RGS localization both qualitatively and quantitatively is observed by deletion of *BNI1*, therefore we sought to better understand the role this formin plays in the pheromone response, as well as how this formin behaves differently from that of Bnr1.

3.8 Bni1 is the Pheromone Responsive Formin and is Necessary for Gradient Tracking

Yeast possess two formins, Bni1 and Bnr1, thought to be functionally redundant, nucleating actin cables to allow filament formation (Karpova et al. 1998; Buttery, Yoshida, and Pellman 2007). The two formins have been shown to localize to different areas in the growing daughter cell during mitosis. The localization of Bnr1 is static, localizing to the bud neck until the end of anaphase, as here it is thought to be filling the mother cell with actin filaments (Buttery, Yoshida, and Pellman 2007). Bni1 on the other hand localizes to the bud neck and forms the polarisome with Bud6, Spa2, and Pea2 at the polar cap of the growing daughter cell (Evangelista et al. 1997; Bidlingmaier and Snyder 2004; Buttery, Yoshida, and Pellman 2007) . These differences in localization, as well as the morphological changes seen upon deleting each

of the formins, led us to hypothesize that Bni1 the pheromone responsive formin, while Bnr1 has roles in mitosis only.

The localization of Bnr1-GFP and Bni1-GFP was assessed using live cell fluorescence imaging both during mitosis and when treated with saturating pheromone (3uM) (Figure 7A). As previously reported, we find Bni1 has a dynamic localization during mitosis, associating with

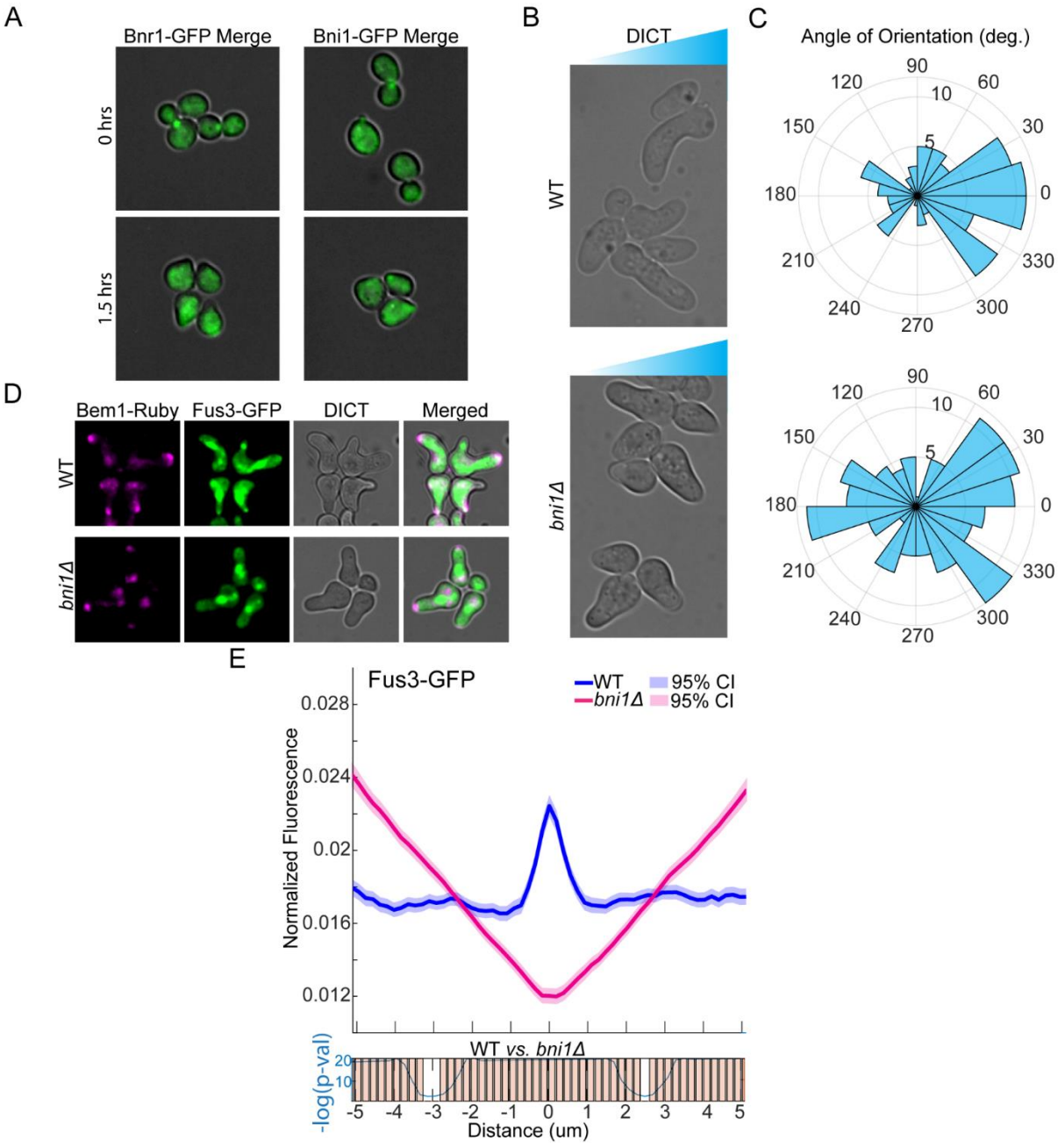

Figure 7. Bni1 is the Pheromone Responsive Formin.

A) Representative images of Bnr1-GFP and Bni1-GFP during mitosis and 1.5hrs in the pheromone response. Bnr1-GFP does not associate to the polar cap during the pheromone response, while Bni1-GFP does. B) Representative DICT images of WT and bni1 cells in a 0-150nM gradient, with the higher concentration of pheromone to the right. C) Rose plots showing the quantification of the final angle of orientation in gradient tracking cells, with 0° being toward the higher levels of pheromone and 180° being away from the pheromone source. Data are derived from n = 95 (WT) and n = 134 (*bni1Δ*). D) Representative images of Fus3-GFP and Bem1-Ruby in WT and *bni1Δ* at time point 6hrs. Deletion of BNI1 results in mislocalization of Fus3-GFP. E) Quantification of the spatial distribution of Fus3-GFP in WT and *bni1Δ* during the course of microfluidics experiment with statistical analysis shown below. Data are derived from n = 2848 (WT) and n = 5394 (*bniΔ*) datapoints per position.

the bud neck and polar cap, while Bnr1 only associates with the bud neck. In response to pheromone treatment, Bni1-GFP localizes to the growing shmoo tip, while Bnr1-GFP has no apparent localization. Additionally, deletion of *BNI1* results in a broadening of shmoos, while deletion of *BNR1* has little effect on the cells ability to shmoo. This leads us to conclude the formin Bni1 is the pheromone responsive formin, needed primarily to nucleate actin at the polarity patch. Through the rest of the study we will focus on the role of Bni1, as opposed to Bnr1, as Bnr1 does not localize during the pheromone response, nor does it affect shmoo morphology.

We hypothesized that deletion of Bni1 would result in a gradient tracking defect compared to that of WT cells because Bni1 has a localization during the pheromone response and is one of the components of the polarisome,. To understand the role Bni1 plays in gradient tracking, we utilized the microfluidics device to set up a pheromone gradient ranging from 0-150nM. Dual fluorescent tagged Sst2-GFP and Bem1-Ruby strains were used in an otherwise WT background as well as in a *bni1Δ* background. Images were taken every 5 min over a 12hr

time course and the angle of orientation of the polar cap was measured in ImageJ for cells present in the central 50% of the chamber at time point 8hrs, before cells began exiting the pheromone response. Representative images are shown in Figure 7B, with the gradient represented by the triangle on top of the images, with the higher concentration of pheromone to the right. Figure 7C shows a rose plot with the angles of orientation at 8 hours into the experiment, with 0° being towards the pheromone gradient, defined as being a tracking cells, and 180° away from the pheromone gradient, defined as non-tracking cells. As shown, cells lacking the formin Bni1 have slight deficiencies in their ability to track a pheromone gradient, with a larger proportion of cells growing away from the pheromone source compared to that of WT (Figure 7C). This defect in gradient tracking allows us to conclude that the formin Bni1 is necessary for cells to properly track a pheromone gradient.

The ability of cells to track a pheromone gradient is due in part to proper endocytosis and exocytosis of vesicles at the growing end of the yeast. Additionally, we propose that the proper localization of Fus3 is affected by the ability to perform endocytosis. Since Bni1 is both the pheromone responsive formin and necessary to perform CIE, we hypothesized that the localization of the Fus3 would be disrupted upon deletion of Bni1. To test this hypothesis, we deleted Bni1 from a dual tagged Fus3-GFP Bem1-Ruby strain and observed the dynamics of Fus3-GFP over 12 hours in a microfluidic chamber. Representative images are shown in Figure 7D of both the WT and *bni1Δ* background with the quantitative analysis of the time course shown in Figure 7E. The ability of Fus3 to form a tight localization is hampered with deletion of *BNI1* (Figure 7D). Through most every point along the cell periphery there is a statistically significant difference in the MAPK localization. From this we can conclude that output through

the formin Bni1 is necessary to localize MAPK during the pheromone response and without the correct localization there is a defect in gradient tracking. In addition to Bni1 being responsible for nucleating actin cables at sites of polarity, it is also responsible for facilitating clathrin independent endocytosis. This led us to pursue the idea that there may be defects in endocytosis in the phosphomimetic Sst2 strain, as this strain also resulted in different localization of MAPK compared to that of WT cells.

3.9 Clathrin Independent Endocytosis is Up-Regulated During the Pheromone Response

Endocytosis allows the internalization of nutrients as well as recycling of materials on the membrane (Raths et al. 1993; Lang et al. 2014; Goode, Eskin, and Wendland 2015). In short, clathrin mediated endocytosis is accomplished through a three-step process in which clathrin binds a selected site, an actin network is set up around the clathrin, and the vesicle is then cleaved off(Goode, Eskin, and Wendland 2015). In terms of the pheromone response, endocytosis of the receptor during the pheromone response regulates signaling through internalization of active receptor (Ballon et al. 2006). Additionally, many of the endocytic events in yeast originate at sites of polarity, while also being needed to maintain the polar patch (Goode, Eskin, and Wendland 2015). Interestingly, yeast, much like most eukaryotic cells, possess means of performing clathrin independent endocytosis (CIE) through the formin Bni1 (Prosser et al. 2011). Clathrin independent endocytosis is positively affected by Rho1 through activation of the formin Bni1 and not Bnr1 (Prosser et al. 2011). The study that came across this discovery found that an additional chemotropic protein was implicated in endocytic pathways, where Kel1, as well as its paralog, Kel2, form a complex with the adapter proteins Pan1 and End3, components that bind to Arp2/3, actin nucleating proteins that form branches

off linear actin, to activate CME (Whitworth et al. 2014). The implication of the proteins Kel1 and Bni1 in affecting the localization of Sst2, as well as the finding that Bni1 is necessary to form tight localization of MAPK, we hypothesized that there was an axis in which the proper localization of Sst2 is necessary to allow clathrin independent endocytosis. Furthermore, phosphorylation of the protein Rvs167 by MAPK inhibits endocytosis through this pathway (Friesen et al. 2003), therefore activation of Bni1, which in turn activates CIE, may be a method to switch modes of endocytosis, depending on the needs of the cell.

To understand the role that endocytosis plays in the pheromone response, we utilized the red fluorescent dye FM4-64 (SynaptoRed), a styryl dye used commonly in yeast systems to track endocytic and lysosomal pathways (Vida and Emr 1995). The styryl portion of the dye is lipophilic enough to allow strong interaction with the outer leaflet of the membrane in low micromolar quantities. Often, the dye is used in pulse-chase experiments, exposing the yeast to FM4-64, briefly washing, then tracking internalization rates and/or localization. For our purposes, we tracked individual cells exposed pheromone (300nM), as well as a continuous flow of 0.6uM FM4-64 in SC media, an order of magnitude lower than that used for single time points. Imaging was performed in 20 min. intervals over a 12hr period. To normalize between errors with abnormal flow due to the dye interacting with the device, the ratio of the amount of internal fluorescence to the amount of external fluorescence was calculated at each time point, as the amount of internalization is dependent on the amount of dye bound to the membrane. A

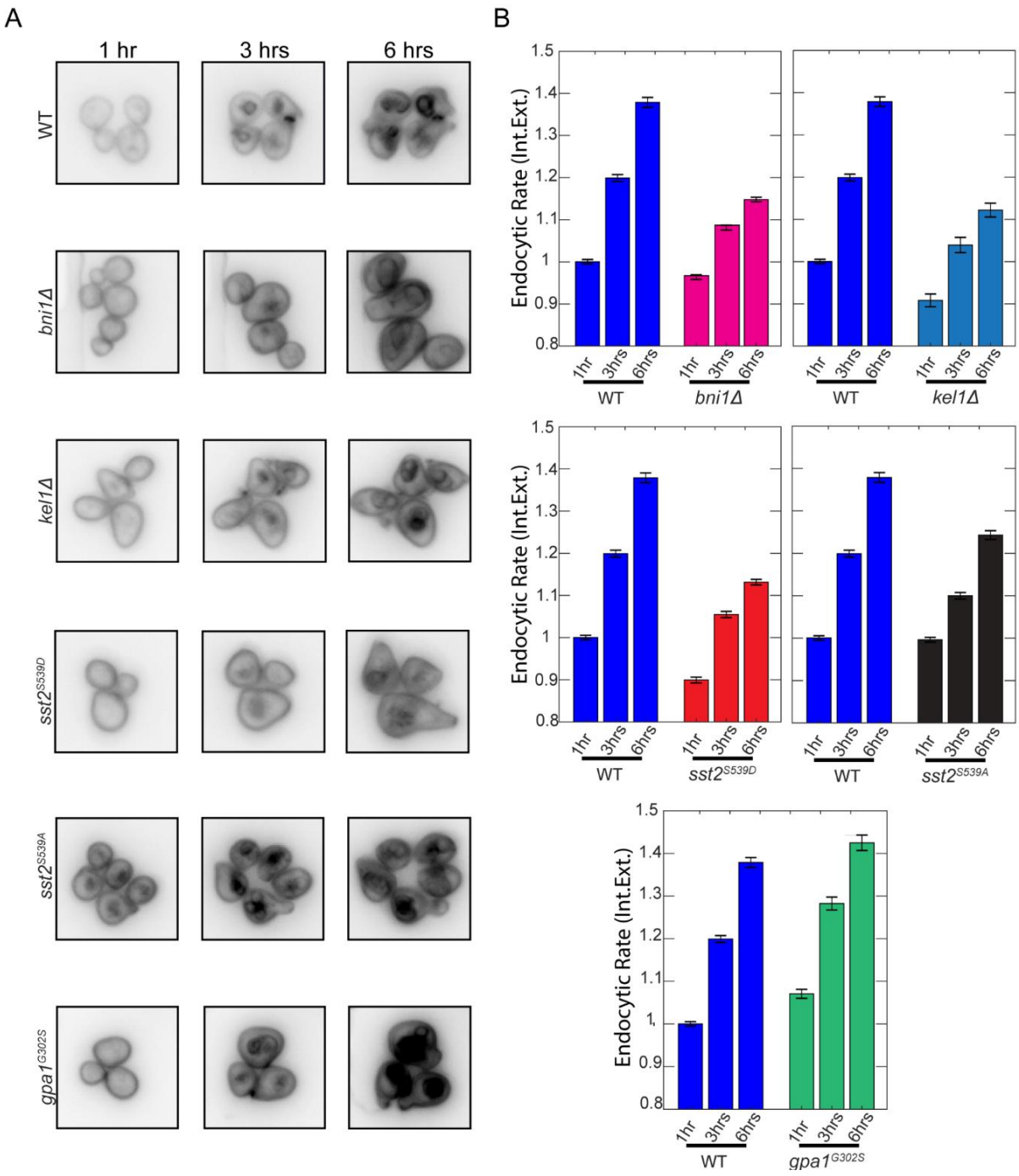

Figure 8. Endocytosis is Affected by the Localization and Activity of RGS

A) Representative images of the internalization of FM4-64 over 6hrs. B) Quantification of endocytosis using the metric of the ratio of internal to external fluorescence over 6hrs. Ratios are plotted vs. strain with standard error of the mean. Data are derived from n = 167 (WT), n = 187 (*bni1Δ*), n = 121 (*kel1Δ*), n =120 ($sst2^{S539D}$), n = 130 ($sst2^{S539A}$), and n = 169 ($gpa1^{G302S}$).

custom MATLAB script was written to define three area of the cell; the whole cell, the internal

cell, and the peripheral cell found by subtracting the whole cell from the internal cell. The average fluorescence intensity for each of the masks was calculated on a cell by cell basis and the ratio of internal to external fluorescence was calculated.

We observed that the continuous addition of the FM4-64 resulted in a subset of cells experiencing toxicity in the later portions of the experiments, noted by a stall in the pheromone response (i.e. discontinuation of all growth). Through the analysis of the ratio of internal to external fluorescence throughout all the time points, we found that strains reached a maximum ratio at about 6hrs into the experiment. For this reason, we quantified the ratios of each strain at time 1hr, 3hrs, and 6hrs, before toxicity in the cells became too high to prevent further signaling. Two independent experiments were quantified to ensure data precision. To establish baseline levels of endocytosis using the metric of internal fluorescence to external fluorescence, we utilized a WT strain with a Sst2-GFP background. As is shown, the WT strain had an early accumulation of FM4-64 on the plasma membrane, though as the experiment progressed, dye accumulated within the vacuole (Figure 8A). The quantification of the ratio of internal to external fluorescence plotted with standard error of the mean, reveals that the dye accumulates more rapidly internally than on the cell periphery, with an average maximum ratio of 1.38 calculated at hour 6 (Figure 8B). This was used as our baseline of normal endocytic processes. It was shown that Bni1 is responsible for clathrin independent endocytosis (Prosser et al. 2011), therefore we utilized the deletion mutant to observe how the levels of internalization would decrease in this mutant. Unsurprisingly, the ratio of internal to external dye was found to be significantly lower than WT upon deleting *BNI1*, averaging 1.15. Accumulation of FM4-64 seen within these mutant yeast is thought to be from other endocytic

pathways, such as CME. This was used as our negative control for endocytosis when comparing other mutant strains.

As we proposed that Bni1 is regulated by the kelch protein Kel1, we sought to determine the levels of endocytosis in this strain. The opposite phenotypes between *kel1Δ* and *bni1Δ* suggested that there may be higher rates of endocytosis in the absence of Kel1, as the cells formed small shmoos, which may be caused by internalizing more material than is being sent to the membrane. Therefore, we hypothesized that without Kel1 around in the cells, the activity of Bni1 would increase and the endocytic rates would increase, resulting in a higher internal to external ratio. Surprisingly, the ratio of internalization upon deleting KEL1 resulted in lower endocytic rates using our metric, measuring at 1.12 at 6hrs (Figure 8B). This may be explained by the fact that the Kelch proteins bind End3 and Pan1, which are adapters for Clathrin mediated endocytosis (Whitworth et al. 2014) and so it may be that the decreased endocytic rates we are observing are due to a defect in the CME pathway.

We hypothesized that the differences in localization of the MAPK seen in the phosphomutants may be due to a defect in endocytosis, in which there is no longer proper endocytosis occurring just adjacent to the polar cap. To address this hypothesis, we looked at the endocytic ratios of internal to external FM4-64 in the phosphomutants. The unphosphorylatable mutant has qualitatively more internal accumulation of the dye compared to that of the phosphomimetic strain (Figure 8A). Quantification of the ratios of dye reveals that both strains have a marked decrease in the rate of endocytosis by time 6hrs, with a ratio of 1.13 for the phosphomimetic and 1.24 for the unphosphorylatable strain (Figure 8B). Notably in the unphosphorylatable strain there is a near equal amount of internalization of that compared to

WT at time point 1hr, with a ratio of 0.99 and 1.0 respectively, while the phosphomimetic mutant is consistently below the levels of the WT strain. From this we were able to conclude that the phosphorylation of Sst2 does decrease endocytic rates. To further tease out if the function and localization of Sst2 is needed to allow proper endocytosis, we observed the *gpa1*^{G302S} mutant, which is not able to be acted upon by Sst2 and results in enhanced localization of Sst2 to the polar cap.

The *gpa1*^{G302S} mutant displays a qualitatively increased amount of accumulation of the FM464 dye (Figure 8A). Throughout each time point observed, the amount of fluorescence internalized was significantly greater than that of WT or any other strain examined. As shown in Figure 8B the maximum ratio of internal to external fluorescence achieved was 1.43 (Figure 8B). Although this number is not greatly different than the WT value, it was higher at all time points quantified. One of the hallmarks of proper chemotropic growth is the ability to control both endocytosis and exocytosis, to both maintain polarity and grow toward the correct source of signal. The hyperactive signaling from the inability of Sst2 to inactivate Gα may lead to an increased activation of the proteins involved in both endocytosis and exocytosis, such as Bni1. These data allow us to conclude that both the localization, through the phosphorylation state of Sst2, as well as the activity of Sst2 are necessary to allow proper endocytosis during the yeast pheromone response.

CHAPTER 4

DISCUSSION AND FUTURE DIRECTIONS

Here we show new consequences of regulation of the main negative regulator of G-Protein Signaling, Sst2. Firstly, we have shown that Sst2 has more nuanced roles within the cell to regulate G-Protein signaling. Sst2 is found to associate dynamically throughout the pheromone response, as it was previously shown to only interact with the receptor and Gα subunit. The most surprising of these localizations was during the early time points of cells exposed to pheromone. During the stages of mitotic exit, it was shown that Sst2 localizes to the bud neck. This association may be necessary to ensure the cells finish mitosis to begin the pheromone response, and thus prevents improper separation of the mother and daughter cells. Previous studies looking at this same localization in the Cdc42 GAP's has found that septins recruit the GAPs to the bud neck to turn off Cdc42 and allow proper septin deposition (Smith et al. 2002; Caviston et al. 2003). This mechanism may be an interesting avenue to study further with Sst2, to verify if it too is necessary at the bud neck to prevent premature signaling through the G-proteins. Evidence found in this study supporting this idea is seen with the deletion of KEL1, which is known to be necessary to prevent early mitotic exit. In this mutant, Sst2-GFP does not localize properly to the bud neck and, whether by action of Sst2 or not, these cells prematurely exit mitosis and begin the pheromone response.

Essential to understanding the function of proteins is to understand their localizations. In this way we have characterized the source of regulation needed for the proper localization of Sst2. To have Sst2 localize correctly during the pheromone response, Sst2 must be able to perform its RGS activity. Removal of Sst2 activity through modifying the Gα subunit prevent

septins, and therefore Sst2-GFP, from localizing to areas peripheral to the polar cap. This consequently results in the cells being unable to track a pheromone gradient and have severe morphological defects, forming globular cells, as opposed to the standard shmooing, pear-like cells. We have additionally found that Sst2 does not have a localization completely coincident with the receptor. To attempt to understand what may be controlling the interaction of Sst2 with both the receptor and Gα subunit, and potentially septins, we characterized a phosphorylation site that was not well understood. Here we showed that the phosphorylation state of Sst2 controls its localization, though it does so in a way that does not affect sensitivity to pheromone. For this reason, we hypothesized that it may affect the localization of other chemotropic proteins and affect pathways less involved in signaling output and more involved in morphology. From this we found that phosphorylation of Sst2 creates a feedback loop that affects the localization for the MAPK. The increased association of the MAPK to areas adjacent to the polar cap in the unphosphorylatable mutant suggested that the removal of Sst2 from its normal binding interactions caused either a lack of removal of an increased delivery of MAPK to the polar cap. For this reason, we turned our attention towards proteins involved in endocytic and exocytic pathways that might also interact with Sst2.

A literature investigation revealed that the formin, Bnr1, and the Kel1 have been shown to interact with Sst2 through a yeast two-hybrid assay. Previous studies in the model S. pombe have found that a Kel1 homologue regulates a Bni1 homolog, and in yeast it has been shown that Kel1 negatively regulates Bnr1 (Martin et al. 2005; Feierbach, Verde, and Chang 2004; Gould et al. 2014). These studies additionally made mention that the formin Bni1 shares a mitotic localization more similar to Kel1 than does Bnr1 (Gould et al. 2014), though they

hypothesized this was due to a stabilization of Bnr1 at the bud neck, and therefore the localization of Kel1 didn't need to be coincident with Bnr1 to perform its regulatory effects. For this reason, we sought to understand the interaction between Kel1 and Bni1, proposing the hypothesis that Kel1 negatively regulate Bni1. Additionally, we sought to understand the interactions between Sst2, Kel1, and the formins, in which Sst2 may be acting as an axis of control of the others. The most obvious question to answer first was to see if deletion of the formins or *KEL1* results in a mitotic localization change of Sst2.

We observed the localization of Sst2 at early timepoints within a microfluidics experiments and saw that Kel1 was necessary to localize Sst2 to the bud neck in cells that are exiting mitosis and beginning the pheromone response. Here we have provided evidence that the defect observed in *kel1Δ* cells may be due to a mislocalization of Sst2. Without Sst2 being present, the activation of the GPCR may proceed prior to exiting mitosis. Further study of this interaction will be necessary to definitively prove the interaction between Sst2 and Kel1 to determine the role in regulating mitotic exit. A proper experiment to determine the interaction would be to express both Sst2 and Kel1 and perform a pulldown or halo assay. Kel1 would have an N-terminal MBP tag used as the bait attached to Maltose beads and Sst2-GFP would be used as prey to identify binding. Since the interaction may be of low affinity, a fluorescence microscopy halo assay would be the most affective, being able to identify high micromolar affinity interactions due to the fact that washing the beads and eluting would not have to be performed. This method may be preferable to standard pulldown assays, as in the cell these proteins may be brought close to one another through other effectors, thereby increasing their local concentration. In this endeavor we are in the process of verifying expression plasmids and

have demonstrated we can express MBP-RGS Domain-GFP fusion protein. Further verification is required to verify the proposed expression plasmids in Table 1 are working as intended, though restriction digests of them all has indicated there is proper insertion of our oligonucleotide of interest.

In deleting each of the formins or *KEL1*, we found that cell morphology and Sst2 localization are least affected by deletion of *BNR1*, where cells are able to form multiple shmoos that are most similar to WT. Additionally, we have shown that deletion of *BNI1* and *KEL1* results in morphologies that are opposite one another, in which cells grow with few, large shmoos with deletion of *BNI1*, and with many small shmoos with deletion of *KEL1*. In both mutants the localization of Sst2 is affected and appears to be more strongly associated in regions of the polar cap. In the case of the *kel1Δ*, we believe the stronger association seen at the polar cap may be due to a smaller separation of the polar cap and septins, due to the smaller shmoo morphology. In the case of *BNI1* deletion, we hypothesize that the larger polar cap association is real, in which it can be qualitatively seen that Sst2 associates there. This leads us to conclude that Bni1 may be necessary to remove Sst2, and that this is in turn is regulated by Kel1 acting on Bni1. Further study will be necessary to prove the direct regulation network between Kel1 and Bni1. Experiments using chimeric proteins of Sst2-Kel and Kel1-Bni1 may be useful to help tease out these interactions. As neither of these proteins are kinases, it is believed that the regulatory interactions may be based on these proteins ability to associate or not during the pheromone response, which may be affect by their phosphorylation state. In these experiments, observing the morphology of cells or looking for readout of the pathway, such as through MAPK localization, may be useful to tease out these interaction networks.

Having shown that Bni1 affects the localization of Sst2 and shmoo morphology, while Bnr1 does not, we examined the roles of Bni1 and Bnr1 in the pheromone response. Previous studies have shown that Bni1 and Bnr1 localize differentially during mitosis, with Bni1 associating with the polar cap, and Bnr1 statically associating at the bud neck. We have shown here that Bni1 is the pheromone responsive formin, as it localizes during the pheromone response, while Bnr1 does not. Additionally, the formin Bni1 is found to be needed for proper gradient tracking, as deletion results in a decreased ability to grow toward the pheromone source. Consequently, the ability of MAPK to localize properly is hampered upon deleting Bni1, leading us to conclude that the ability of Bni1 to facilitate endocytosis is necessary to polarize MAPK correctly, which may be through proper endocytic events.

Data shown here points to a mechanism in which the localization of the MAPK is controlled through the phosphorylation state of Sst2, the ability of MAPK to bind Gα, as well as activity of Bni1. We propose that Gα control of MAPK allows proper CIE by regulating the localization of Sst2, thereby controlling its binding interactions with proteins involved in endocytosis. For this reason, we examined the endocytic rates in a number of strains and found that phosphorylation of Sst2 reduces endocytosis compared to that of WT and was reduced to levels seen in a *bni1Δ*. Interestingly, the unphosphorylatable mutant has lower levels of endocytosis compared to that of WT, though the levels were still above that of the phosphomimetic strain. This deviation from WT behavior in the unphosphorylatable strain may be explained through one of our earlier hypotheses. We proposed that RGS interaction with Kel1 was necessary to allow the proper control of Bni1, and that this interaction was controlled through phosphorylation of Sst2, in which the unphosphorylatable form was able to interact

with Kel1 and the phosphomimetic form was not. Surprisingly, endocytosis rates in a *KEL1* deletion are seen to be low, much like that seen in *bni1Δ* mutants. The low *kel1Δ* endocytic rates, which were initially surprising, may be due to the interactions of Kel1 with the CME adapter protein, End3, which forms a complex with Arp2/3 (Whitworth et al. 2014). In this way, Kel1 may be found at an axis in which it shuts down CIE through Bni1, to allow CME to predominate. The need for this source of regulation may be due to the dynamic state of the yeast pheromone response. Recycling of material on the cell periphery and movement of the polar cap by creating a "vacuum", may be enabled by CIE, while targeted uptake of pheromone responsive proteins, such as active receptor, is accomplished through Clathrin mediated pathways. The dynamic control of this type of system would require multiple feedback mechanisms and dynamic regulation to allow proper gradient tracking with a relatively small subset of proteins, proposed to be at an axis between MAPK, Sst2, Bni1, and Kel1. In conclusion, this study has provided evidence for a new and exciting regulatory role of Sst2 in limiting endocytosis during the yeast pheromone response.

Table 1. Yeast Strains

Strain	Parent	Description
BY4741		*Mata leu2Δ met15Δ his3Δ ura3Δ*
SST2-GFP	BY4741	*SST2-GFP::HIS3*
SST2-GFP BEM1-RUBY2	BY4741	*SST2-GFP::HIS3 BEM1-RUBY2::KanMX4*
SST2^{S539A}	BY4741	*sst2^{S539A}*
SST2^{S539A}-GFP BEM1-RUBY2	BY4741	*sst2^{S539A}-GFP::URA3 BEM1-RUBY2::KanMX4*
SST2^{S539D}-GFP	BY4741	*sst2^{S539D}-GFP::HIS3*
SST2^{S539D}-GFP BEM1-RUBY2	BY4741	*sst2^{S539D}-GFP::HIS3 BEM1-RUBY2:LEU2*
KEL1Δ SST2^{S539D}-GFP	BY4741	*kel1Δ::KanMX4 SST2^{S539D}-GFP::HIS3*
KEL1Δ SST2-GFP	BY4741	*kel1Δ::KanxMX4 SST2-GFP::HIS3*
KEL1Δ SST2-GFP BEM1-RUBY2	BY4741	*kel1Δ::KanMX4 SST2-GFP::HIS3 BEM1-RUBY2::LEU2*
KEL1Δ FUS3-GFP BEM1-RUBY2	BY4741	*kel1Δ::KanMX4 FUS3-GFP::HIS3 BEM1-RUBY2::LEU2*
GPA1^{G302S}	BY4741	*gpa1^{G302S}::URA3*
GPA1^{G302S} SST2-GFP BEM1-RUBY2	BY4741	*gpa1^{G302S}::URA3 SST-GFP::HIS3 Bem1-RUBY2::LEU2*
GPA1^{EE} SST2-GFP BEM1-RUBY2	BY4741	*gpa1^{EE}::URA3 SST-GFP::HIS3 Bem1-RUBY2::LEU2*
GPA1^{EE} FUS3-GFP BEM1-RUBY2	BY4741	*gpa1^{EE}::URA3 FUS3-GFP::HIS3 Bem1-RUBY2::LEU2*
BEM3Δ GPA1^{G302S} SNC2-GFP	BY4741	*bem3Δ::KanMX4 gpa1^{G302S}::URA3 SNC2-GFP::HIS3*
BNI1Δ SST2-GFP	BY4741	*bni1Δ::KanMX4 SST2-GFP::HIS3*
BNI1Δ SST2-GFP BEM1-RUBY	BY4741	*bni1Δ::KanMX4 SST2-GFP::HIS3 BEM1-RUBY2::LEU2*
BNI1Δ FUS3-GFP BEM1-RUBY	BY4741	*bni1Δ::KanMX4 SST2-GFP::HIS3 BEM1-RUBY2::LEU2*
BNR1Δ SST2-GFP	BY4741	*bnr1Δ::KAnMX4 SST2-GFP::HIS3*
BNR1Δ SST2-GFP BEM1-RUBY2	BY4741	*bnr1Δ::KAnMX4 SST2-GFP::HIS3 BEM1-RUBY::LEU2*
FUS3-GFP BEM1-RUBY2	BY4741	*FUS3-GFP::HIS3 BEM1-RUBY2::LEU2*
SST2^{S539A} FUS3-GFP BEM1-RUBY2	BY4741	*sst2^{S539A} FUS3-GFP::HIS3 BEM1-RUBY2::LEU2*
SST2^{S539A} STE2-GFP BEM1-RUBY2	BY4741	*sst2^{S539A} STE2-GFP::HIS3 BEM1-RUBY2::LEU2*
SST2^{S539D} FUS3-GFP BEM1-RUBY2	BY4741	*sst2^{S539D} FUS3-GFP::HIS3 BEM1-RUBY2:LEU2*
SST2^{S539D} STE2-GFP BEM1-RUBY2	BY4741	*sst2^{S539D} STE2-GFP::HIS3 BEM1-RUBY2::LEU2*

Table 2. Plasmids

Plasmid	Vector	Description
pFA6a-yomEGFP-His	pFA6a	Tagging of EGFP-His
pFA6a-yomEGFP-Kan	pFA6a	Tagging of EGFP-Kan
pFA6a-yomRuby2-His	pFA6a	Tagging of Ruby-His
pFA6a-yomRuby2-Kan	pFA6a	Tagging of Ruby-Kan
pFA6a-yomRuby2-Leu	pFA6a	Tagging of Ruby-Leu
pRSII405-Bem1-Ruby2	pRSII405	Integrating BEM1-RUBY::LEU2 Vector
pRSII406-gpa1^{G302S}	pRSII406	Integrating *gpa1*^{G302S}::URA3 Vector
pRS406-sst2-GFP	pRSII406	Integrating SST2-GFP::URA3 Vector
PRSII406-sst2^{S539A}-GFP	pRSII406	Integrating *sst2*^{S539A}-GFP::URA3 Vector
pMAL-TEV -SST2-GFP-c5X	pMAL c5X	Expression pMAL-TEV-SST2-GFP-c5X
pMAL-TEV -SST2^{S539A}-GFP-c5X	pMAL c5X	Expression pMAL-TEV-*sst2*^{S539A}-GFP-c5X
pMAL-TEV-SST2^{S539D}-GFP-c5X	pMAL c5X	Expression pMAL-TEV-*sst2*^{S539D}-GFP-c5X
pMAL-TEV-RGS-GFP-c5X	pMAL c5X	Expression pMAL-TEV-RGS-GFP-c5X
pMAL-KEL1-c5X	pMAL c5X	Expression pMAL-KEL1-c5X

pFA6a plasmids were a gift from Wendell Lim & Kurt Thorn

Table 3. Primers

OLIGONUCL-EOTIDE NAME	SEQUENCE	GENE	DESCRIPTION
AHM-8	5' TTTGACGAATTCTAAGACCAAACTGAGTAG AAGC 3'	GPA1	FP for copying GPA1 with EcoRI cut site
AHM-18	5' gcatcagtctagaCCATCATAGACTCTAATGGAG AAG 3'	GPA1	RP for copying GPA1 with XbaI cut site
AHM-26	5' TCTACAGAACgAAgagGCCAATGATGTCATC 3'	GPA1	FP for mutagenesis for GPA1 EE, Primer from NEB
AHM-27	5' AAAGGATCACTTTCGTCTC 3'	GPA1	RP for mutagenesis for GPA1 EE, Primer from NEB
AHM-28	5' GTAGGAAATAcTGGGGTGTACAG 3'	GPA1	FP for mutagenesis of Start codon ATG to CTG in GPA1
AHM-29	5' CTTAATATATCAATTTATACACCTC 3'	GPA1	RP for mutagenesis of Start codon ATG to CTG in GPA1
AHM-32	5' AAAGACTACAaGCATTACAGAAAC 3'	GPA1	FP 60 bp (40 addition to) PCR for pCORE into GPA1
AHM-33	5' ATACGGCCCTTCAAAATG 3'	GPA1	RP 60 bp (40 addition to) PCR for pCORE into GPA1
AHM-22	GATGCGGTTTTTTACAGGGC	FUS3	FP for copying FUS3, Primer from Yeast Genome Database
AHM-23	ATGGATCACCCCTTGTGGTTCT	FUS3	RP for copying FUS3, Primer from Yeast Genome Database
JKM-16	CATAATCCAAGCCAAACTGAAAATTTCCG TTCACGATATTGGTGACGGTGCTGGTTTA	BEM1	Forward primer pFA6a labeling for BEM1

Table 3. Continued

JKM-17	CAAGTAAAGAAGAAAAATGCTTCGTCTTC TAACACTAGATTCGATGAATTCGAGCTCG	BEM1	Reverse primer pFA6a labeling for BEM1
JKM-18	GTCTGCGAATTCGGTGACGGTGCTGGTTT AAT	yomRUBY 2	EcoRI Ruby2 primer for cloning into pRSII405 with Bem1
JKM-19	CGTAGCTCTAGATTACTTATACAATTCAT CCA	yomRUBY 2	XbaI Ruby2 reverse primer for cloning into pRSII405 with Bem1
JKM-20	CTGAACGGTACCGACAACTTATGTGGGAG AGA	BEM1	KpnI-Bem1 primer for cloning into pRSII405
JKM-21	CGTACCGAATTCAATATCGTGAACGGAAA TTT	BEM1	
JKM-28	ATATGCGGCCGCGAGAATTTGTATTTTCA GGGTGTGGATAAAAATAGGACGTT	SST2	Not1-TEV-Sst2 5' (no ATG) primer for cloning into pMAL c5X
JKM-29	ATATGCGGCCGCGAGAATTTGTATTTTCA GGGTAATTTAAATAAACTGGACTA	SST2 RGS DOMAIN	Not1-TEV-sst2 RGS domain 5' primer for cloning into pMAL c5X
JKM-30	TTGCGTTGATAGATTATGTAGGAATTCTT ACTTGTATAATTCATCCAT	yo-EGFP	yo-eGFP 3'-EcoRI-shuffledTEV primer for cloning into pMAL c5X
JKM-31	ATATGCGGCCGCGCTGGATTCAGCTTCGC CAAG	KEL1	Not1-Kel1 5' primer (no ATG) for cloning into pMAL c5X

Table 3. Continued

JKM-33	ATATGCGGCCGCGGTAGGAGGGCTTTTGTAGAA	yomRUBY2	NotI-Ruby 5' (no ATG) primer for cloning into pMAL c5X
JKM-34	GCGCGAATTCTTACAACACTCCCTTCGTGCT	yomRUBY2	Ruby 3'- EcoRI primer for cloning into pMAL c5X
RTM-5	CAAAGATGCTAGCGCTTTAATAGAAATCCAAGAAAAGTGCGGTGACGGTGCTGGTTTA	SST2	Forward primer pFA6a yo-tagging for Sst2
RTM-6	GTGCAATTGTACCTGAAGATGAGTAAGACTCTCAATGAAATCGATGAATTCGAGCTCG	SST2	Reverse primer pFA6a yo-tagging for Sst2
SSM-1	AGAGAGAACGCATGCTATGCTGAACGATATTCAAAATATAGGTGACGGTGCTGGTTTA	BNR1	amplifies pFA6a with homology to Bnr1 for labeling
SSM-2	TTATATAAGCTCCACAACTACATAAAATACTAAGTCTTCATCGATGAATTCGAGCTCG	BNR1	amplifies pFA6a with homology to Bnr1 for labeling
SSM-3	GTGCCAAGGAAAACATTGA	BNR1	for verifying tag of BNR 3'
SSM-4	ACAGACACATTGCCCATCTT	BNR1	for verifying tag of BNR 3'
SSM-5	TGCCACAAGGGGTGTTATGAA	BNI1	amplifies GFP
SSM-6	TCAGCGAACGCGAAATACAA	BNI1	amplifies GFP
SSM-7	ACCCATCTTCCGCCAGAAA	BNI1	for verifying tag of BNI 3'
SSM-8	TGTTTATCCACGCTCTCGAT	BNI1	for verifying tag of BNI 3'
SVM-17	GAACTTTACAACTTGTACCCTTCATCACCT	KEL1	Deletion cassette (250 bp out)

Table 3. Continued

SVM-18	GCACCGCCCAAATACTGCAATCGGACTATTCTGCG	KEL1	Deletion cassette (250 bp out)
SVM-21	ACTGGACGTACGATGGTGTT	KEL1	Deletion verification cassette (500 bp)
SVM-22	CGAACAGCTTCAACGTACCT	KEL1	Deletion verification cassette (500 bp)
SVM-25	CACCAAACAAGTTAATGAAGATGCTGACAGCGATCTACTAGGTGACGGTGCTGGTTTA	KEL1	Kel1 with pFA6a labelling
SVM-26	TTACACATGAAAAGTGAAATTTCATTACGCATATTGTCTTTCGATGAATTCGAGCTCG	KEL1	Kel1 with pFA6a labelling
WSM-7	GGAAGCCAGAAAGTTCTGGACTGAAGATAATAATAATTTAGGTGACGGTGCTGGTTTA	STE2	Forward primer pFA6a yo-tagging for Ste2
WSM-8	GAAGGTCACGAAATTACTTTTTCAAAGCCGTAAATTTTGATCGATGAATTCGAGCTCG	STE2	Forward primer pFA6a yo-tagging for Ste2
WSM-11	GATGCTAAAAGCAGTCTCAG	STE2	Forward primer STE2 c-terminal tag verification
WSM-12	GAGAGTTCTAGATCATGGCA	STE2	Reverse primer STE2 c-terminal tag verification
WSM-13	ATCATGTTGCACCCTCATTC	SST2	Forward primer SST2 c-terminal tag verification
WSM-14	GAATGAATTTGCGTTCAATC	SST2	Reverse primer SST2 c-terminal tag verification

Table 3. Continued

WSM-21	TCCATCATAACTTGCGTCAGAATATTTCTGACATCATGTTGCACCCTCATGAGCTCGTTTTCGACACTGG	SST2	Insert pCORE at sst2 s539
WSM-22	GATGCAGGTGATGGATCGTATAGATTAGTAGGAAAGTGTTCCGATAATGGTCCTTACCATTAAGTTGATC	SST2	Insert pCORE at sst2 s539
WSM-23	TGCGTCAGAATATTTCTGACATCATGTTGCACCCTCATGCTCCATTATCGGAACACTTTCCTACTAATCTATACGATCCA	SST2	S539A mutagenesis with pCORE
WSM-24	TGGATCGTATAGATTAGTAGGAAAGTGTTCCGATAATGGAGCATGAGGGTGCAACATGATGTCAGAAATATTCTGACGCA	SST2	S539A mutagenesis with pCORE
WSM-28	ATGCATGGATCCGTGCTTATAACTTTAAGAAAAACCAGCGTC	SST2	With Kpn1 cut-site for creation of integrating vector
WSM-29	ATGCATGGTACCGCCGGTAGAGGTGTGGTCAATAA	SST2	With BamHI cut-site for creation of integrating vector
WSM-37	GCACCCTCATGCTCCATTATCGG	SST2	Creation of S539A with Q5
WSM-38	AACATGATGTCAGAAATATTCTGACG	SST2	Creation of S539A with Q5
WSM-44	ACACTGAGATTATAGTCCAG	SST2	Verify Sst2 Integration Vector, Binds upstream of sst2
WSM-45	TACTATACCTGAGAAAGCAA	SST2	Verify Sst2 Integration Vector,
WSM-46	TGCGTCAGAATATTTCTGACATCATGTTGCACCCTCATGATCCATTATCGGAACACTTTCCTACTAATC	SST2	Creation of Sst2 S539D from pCORE KO

Table 3. Continued

WSM-46	TGGATCGTATAGATTAGTAGGAAAGTGTTCCGATAATGGATCATGAGGGTGCAACATGATGTCAGAA	SST2	Creation of Sst2 S539D from pCORE KO
WSM-52	GTACTCAGAGCCACAAGAAA	BNR1	amplify bnr1 del insert
WSM-53	CCCGATGAACTCATTGAGAA	BNR1	verify bnr1 deleted
WSM-54	CTAGCGTTCAATTGCCTTCT	BNR1	verify bnr1 deleted
WSM-55	CTGACGGCTGTGTGTTAATT	BNI1	amplify bni1 del insert
WSM-56	AGCGAACGCGAAATACAAGT	BNI1	amplify bni1 del insert
WSM-57	CCAAATCCTTGCTCAACTCT	BNI1	verify bni1 deleted
WSM-62	ACGAAATGACACGCTTGTGA	KEL2	Pairs with WSM 64 KEL2 Del and GFP Tagging
WSM-63	CGTCAAGGACGAAATTCACA	KEL2	Pairs with WSM 65 Kel2 Deletion and GFP tagging verify.
WSM-64	ACAGTTTCGCTTCGTTAAGG	KEL2	Pairs with WSM 62
WSM-65	CCAACATGGTGACTGTCATT	KEL2	Pairs with WSM 63
WSM-70	TGTGGAGGAAACCATCAAGA	LEU2	Verify Internal Leu2
WSM-82	CTAGTGGTAATTATCGTTCCTATCGTCGTCCATTTCAGCGGTGACGGTGCTGGTTTA	SNC2	pfa6 labeling SNC2
WSM-83	TATATATTTTTTAGAATTAGCATCGGGAACCGATGAGCGGAATTCGAGCTCGTTTAAAC	SNC2	pfa6 labeling SNC2
WSM-84	ACGGTGGGAATAATGAGAGA	SNC2	amplify genomic region
WSM-85	GGCGCGAGAAACAAAATTGT	SNC2	amplify genomic region

BIBLIOGRAPHY

1. Alvaro, C. G., and J. Thorner. 2016. 'Heterotrimeric G Protein-coupled Receptor Signaling in Yeast Mating Pheromone Response', *J Biol Chem*, 291: 7788-95.

2. Apanovitch, D. M., T. Iiri, T. Karasawa, H. R. Bourne, and H. G. Dohlman. 1998. 'Second site suppressor mutations of a GTPase-deficient G-protein alpha-subunit. Selective inhibition of Gbeta gamma-mediated signaling', *J Biol Chem*, 273: 28597-602.

3. Arkowitz, R. A. 2009. 'Chemical gradients and chemotropism in yeast', *Cold Spring Harb Perspect Biol*, 1: a001958.

4. Ballon, D. R., P. L. Flanary, D. P. Gladue, J. B. Konopka, H. G. Dohlman, and J. Thorner. 2006. 'DEP-domain-mediated regulation of GPCR signaling responses', *Cell*, 126: 1079-93.

5. Berrie, C. P., N. J. Birdsall, A. S. Burgen, and E. C. Hulme. 1979. 'Guanine nucleotides modulate muscarinic receptor binding in the heart', *Biochem Biophys Res Commun*, 87: 1000-5.

6. Bi, E., and H. O. Park. 2012. 'Cell polarization and cytokinesis in budding yeast', *Genetics*, 191: 347-87.

7. Bidlingmaier, S., and M. Snyder. 2004. 'Regulation of polarized growth initiation and termination cycles by the polarisome and Cdc42 regulators', *J Cell Biol*, 164: 207-18.

8. Buck, L., and R. Axel. 1991. 'A novel multigene family may encode odorant receptors: a molecular basis for odor recognition', *Cell*, 65: 175-87.

9. Burchett, S. A., P. Flanary, C. Aston, L. Jiang, K. H. Young, P. Uetz, S. Fields, and H. G. Dohlman. 2002. 'Regulation of stress response signaling by the N-terminal dishevelled/EGL-10/pleckstrin domain of Sst2, a regulator of G protein signaling in Saccharomyces cerevisiae', *J Biol Chem*, 277: 22156-67.

10. Buttery, S. M., S. Yoshida, and D. Pellman. 2007. 'Yeast formins Bni1 and Bnr1 utilize different modes of cortical interaction during the assembly of actin cables', *Mol Biol Cell*, 18: 1826-38.

11. Butty, A. C., N. Perrinjaquet, A. Petit, M. Jaquenoud, J. E. Segall, K. Hofmann, C. Zwahlen, and M. Peter. 2002. 'A positive feedback loop stabilizes the guanine-nucleotide exchange factor Cdc24 at sites of polarization', *EMBO J*, 21: 1565-76.

12. Caldwell, G. A., F. Naider, and J. M. Becker. 1995. 'Fungal lipopeptide mating pheromones: a model system for the study of protein prenylation', *Microbiol Rev*, 59: 406-22.

13. Caviston, J. P., M. Longtine, J. R. Pringle, and E. Bi. 2003. 'The role of Cdc42p GTPase-activating proteins in assembly of the septin ring in yeast', *Mol Biol Cell*, 14: 4051-66.
14. Chen, R. E., J. C. Patterson, L. S. Goupil, and J. Thorner. 2010. 'Dynamic localization of Fus3 mitogen-activated protein kinase is necessary to evoke appropriate responses and avoid cytotoxic effects', *Mol Cell Biol*, 30: 4293-307.

15. DiBello, P. R., T. R. Garrison, D. M. Apanovitch, G. Hoffman, D. J. Shuey, K. Mason, M. I. Cockett, and H. G. Dohlman. 1998. 'Selective uncoupling of RGS action by a single point mutation in the G protein alpha-subunit', *J Biol Chem*, 273: 5780-4.

16. Dixit, G., J. B. Kelley, J. R. Houser, T. C. Elston, and H. G. Dohlman. 2014. 'Cellular noise suppression by the regulator of G protein signaling Sst2', *Mol Cell*, 55: 85-96.

17. Dohlman, H. G., J. Song, D. Ma, W. E. Courchesne, and J. Thorner. 1996. 'Sst2, a negative regulator of pheromone signaling in the yeast Saccharomyces cerevisiae: expression, localization, and genetic interaction and physical association with Gpa1 (the G-protein alpha subunit)', *Mol Cell Biol*, 16: 5194-209.

18. Dohlman, H. G., and J. Thorner. 1997. 'RGS proteins and signaling by heterotrimeric G proteins', *J Biol Chem*, 272: 3871-4.

19. Dohlman, H. G., J. Thorner, M. G. Caron, and R. J. Lefkowitz. 1991. 'Model systems for the study of seven-transmembrane-segment receptors', *Annu Rev Biochem*, 60: 653-88.

20. Dohlman, H. G., and J. W. Thorner. 2001. 'Regulation of G protein-initiated signal transduction in yeast: paradigms and principles', *Annu Rev Biochem*, 70: 703-54.

21. Dyer, J. M., C. D. Cornellison, A. J. Grosvenor, S. Clerens, and S. Deb-Choudhury. 2014. 'Molecular marker approaches for tracking redox damage and protection in keratins', *J Cosmet Sci*, 65: 25-36.

22. Elion, E. A. 2001. 'The Ste5p scaffold', *J Cell Sci*, 114: 3967-78.

23. Elion, E. A., B. Satterberg, and J. E. Kranz. 1993. 'FUS3 phosphorylates multiple components of the mating signal transduction cascade: evidence for STE12 and FAR1', *Mol Biol Cell*, 4: 495-510.

24. Errede, B., L. Vered, E. Ford, M. I. Pena, and T. C. Elston. 2015. 'Pheromone-induced morphogenesis and gradient tracking are dependent on the MAPK Fus3 binding to Galpha', *Mol Biol Cell*, 26: 3343-58.

25. Evangelista, M., K. Blundell, M. S. Longtine, C. J. Chow, N. Adames, J. R. Pringle, M. Peter, and C. Boone. 1997. 'Bni1p, a yeast formin linking cdc42p and the actin cytoskeleton during polarized morphogenesis', *Science*, 276: 118-22.

26. Feierbach, B., F. Verde, and F. Chang. 2004. 'Regulation of a formin complex by the microtubule plus end protein tea1p', *J Cell Biol*, 165: 697-707.

27. Friesen, H., K. Murphy, A. Breitkreutz, M. Tyers, and B. Andrews. 2003. 'Regulation of the yeast amphiphysin homologue Rvs167p by phosphorylation', *Mol Biol Cell*, 14: 3027-40.

28. Gardner, J. M., and S. L. Jaspersen. 2014. 'Manipulating the yeast genome: deletion, mutation, and tagging by PCR', *Methods Mol Biol*, 1205: 45-78.

29. Garrison, T. R., D. M. Apanovitch, and H. G. Dohlman. 2002. 'Purification of RGS protein, Sst2, from Saccharomyces cerevisiae and Escherichia coli', *Methods Enzymol*, 344: 632-47.

30. Garrison, T. R., Y. Zhang, M. Pausch, D. Apanovitch, R. Aebersold, and H. G. Dohlman. 1999. 'Feedback phosphorylation of an RGS protein by MAP kinase in yeast', *J Biol Chem*, 274: 36387-91.

31. Giot, L., and J. B. Konopka. 1997. 'Functional analysis of the interaction between Afr1p and the Cdc12p septin, two proteins involved in pheromone-induced morphogenesis', *Mol Biol Cell*, 8: 987-98.

32. Gold, S. J., Y. G. Ni, H. G. Dohlman, and E. J. Nestler. 1997. 'Regulators of G-protein signaling (RGS) proteins: region-specific expression of nine subtypes in rat brain', *J Neurosci*, 17: 8024-37.

33. Goode, B. L., J. A. Eskin, and B. Wendland. 2015. 'Actin and endocytosis in budding yeast', *Genetics*, 199: 315-58.

34. Gould, C. J., M. Chesarone-Cataldo, S. L. Alioto, B. Salin, I. Sagot, and B. L. Goode. 2014. 'Saccharomyces cerevisiae Kelch proteins and Bud14 protein form a stable 520-kDa formin regulatory complex that controls actin cable assembly and cell morphogenesis', *J Biol Chem*, 289: 18290-301.

35. Gulli, M. P., M. Jaquenoud, Y. Shimada, G. Niederhauser, P. Wiget, and M. Peter. 2000. 'Phosphorylation of the Cdc42 exchange factor Cdc24 by the PAK-like kinase Cla4 may regulate polarized growth in yeast', *Mol Cell*, 6: 1155-67.

36. Haber, J. E. 2012. 'Mating-type genes and MAT switching in Saccharomyces cerevisiae', *Genetics*, 191: 33-64.

37. Hao, N., S. Nayak, M. Behar, R. H. Shanks, M. J. Nagiec, B. Errede, J. Hasty, T. C. Elston, and H. G. Dohlman. 2008. 'Regulation of cell signaling dynamics by the protein kinase-scaffold Ste5', *Mol Cell*, 30: 649-56.

38. Herskowitz, I. 1988. 'Life cycle of the budding yeast Saccharomyces cerevisiae', *Microbiol Rev*, 52: 536-53.

39. Hofken, T., and E. Schiebel. 2002. 'A role for cell polarity proteins in mitotic exit', *EMBO J*, 21: 4851-62.

40. Huh, W. K., J. V. Falvo, L. C. Gerke, A. S. Carroll, R. W. Howson, J. S. Weissman, and E. K. O'Shea. 2003. 'Global analysis of protein localization in budding yeast', *Nature*, 425: 686-91.

41. Hung, W., K. A. Olson, A. Breitkreutz, and I. Sadowski. 1997. 'Characterization of the basal and pheromone-stimulated phosphorylation states of Ste12p', *Eur J Biochem*, 245: 241-51.
42. Jenness, D. D., and P. Spatrick. 1986. 'Down regulation of the alpha-factor pheromone receptor in S. cerevisiae', *Cell*, 46: 345-53.

43. Kaksonen, M., and A. Roux. 2018. 'Mechanisms of clathrin-mediated endocytosis', *Nat Rev Mol Cell Biol*, 19: 313-26.

44. Karpova, T. S., J. G. McNally, S. L. Moltz, and J. A. Cooper. 1998. 'Assembly and function of the actin cytoskeleton of yeast: relationships between cables and patches', *J Cell Biol*, 142: 1501-17.

45. Kelley, J. B., G. Dixit, J. B. Sheetz, S. P. Venkatapurapu, T. C. Elston, and H. G. Dohlman. 2015. 'RGS proteins and septins cooperate to promote chemotropism by regulating polar cap mobility', *Curr Biol*, 25: 275-85.

46. Kraakman, L., K. Lemaire, P. Ma, A. W. Teunissen, M. C. Donaton, P. Van Dijck, J. Winderickx, J. H. de Winde, and J. M. Thevelein. 1999. 'A Saccharomyces cerevisiae G-protein coupled receptor, Gpr1, is specifically required for glucose activation of the cAMP pathway during the transition to growth on glucose', *Mol Microbiol*, 32: 1002-12.

47. Lang, M. J., J. Y. Martinez-Marquez, D. C. Prosser, L. R. Ganser, D. Buelto, B. Wendland, and M. C. Duncan. 2014. 'Glucose starvation inhibits autophagy via vacuolar hydrolysis and induces plasma membrane internalization by down-regulating recycling', *J Biol Chem*, 289: 16736-47.

48. Leberer, E., D. Dignard, D. Harcus, D. Y. Thomas, and M. Whiteway. 1992. 'The protein kinase homologue Ste20p is required to link the yeast pheromone response G-protein beta gamma subunits to downstream signalling components', *EMBO J*, 11: 4815-24.

49. Lee, S., W. A. Lim, and K. S. Thorn. 2013. 'Improved blue, green, and red fluorescent protein tagging vectors for S. cerevisiae', *PLoS One*, 8: e67902.

50. Longtine, M. S., H. Fares, and J. R. Pringle. 1998. 'Role of the yeast Gin4p protein kinase in septin assembly and the relationship between septin assembly and septin function', *J Cell Biol*, 143: 719-36.

51. Maeder, C. I., M. A. Hink, A. Kinkhabwala, R. Mayr, P. I. Bastiaens, and M. Knop. 2007. 'Spatial regulation of Fus3 MAP kinase activity through a reaction-diffusion mechanism in yeast pheromone signalling', *Nat Cell Biol*, 9: 1319-26.

52. Martin, S. G., W. H. McDonald, J. R. Yates, 3rd, and F. Chang. 2005. 'Tea4p links microtubule plus ends with the formin for3p in the establishment of cell polarity', *Dev Cell*, 8: 479-91.

53. Matheos, D., M. Metodiev, E. Muller, D. Stone, and M. D. Rose. 2004. 'Pheromone-induced polarization is dependent on the Fus3p MAPK acting through the formin Bni1p', *J Cell Biol*, 165: 99-109.

54. McClure, A. W., M. Minakova, J. M. Dyer, T. R. Zyla, T. C. Elston, and D. J. Lew. 2015. 'Role of Polarized G Protein Signaling in Tracking Pheromone Gradients', *Dev Cell*, 35: 471-82.

55. Metodiev, M. V., D. Matheos, M. D. Rose, and D. E. Stone. 2002. 'Regulation of MAPK function by direct interaction with the mating-specific Galpha in yeast', *Science*, 296: 1483-6.

56. Moseley, J. B., I. Sagot, A. L. Manning, Y. Xu, M. J. Eck, D. Pellman, and B. L. Goode. 2004. 'A conserved mechanism for Bni1- and mDia1-induced actin assembly and dual regulation of Bni1 by Bud6 and profilin', *Mol Biol Cell*, 15: 896-907.

57. Nern, A., and R. A. Arkowitz. 1999. 'A Cdc24p-Far1p-Gbetagamma protein complex required for yeast orientation during mating', *J Cell Biol*, 144: 1187-202.

58. Ogura, K., T. Tandai, S. Yoshinaga, Y. Kobashigawa, H. Kumeta, T. Ito, H. Sumimoto, and F. Inagaki. 2009. 'NMR structure of the heterodimer of Bem1 and Cdc24 PB1 domains from Saccharomyces cerevisiae', *J Biochem*, 146: 317-25.

59. Prosser, D. C., T. G. Drivas, L. Maldonado-Baez, and B. Wendland. 2011. 'Existence of a novel clathrin-independent endocytic pathway in yeast that depends on Rho1 and formin', *J Cell Biol*, 195: 657-71.

60. Raths, S., J. Rohrer, F. Crausaz, and H. Riezman. 1993. 'end3 and end4: two mutants defective in receptor-mediated and fluid-phase endocytosis in Saccharomyces cerevisiae', *J Cell Biol*, 120: 55-65.

61. Roberts, C. J., B. Nelson, M. J. Marton, R. Stoughton, M. R. Meyer, H. A. Bennett, Y. D. He, H. Dai, W. L. Walker, T. R. Hughes, M. Tyers, C. Boone, and S. H. Friend. 2000. 'Signaling and circuitry of multiple MAPK pathways revealed by a matrix of global gene expression profiles', *Science*, 287: 873-80.

62. Sadian, Y., C. Gatsogiannis, C. Patasi, O. Hofnagel, R. S. Goody, M. Farkasovsky, and S. Raunser. 2013. 'The role of Cdc42 and Gic1 in the regulation of septin filament formation and dissociation', *Elife*, 2: e01085.

63. Schindelin, J., I. Arganda-Carreras, E. Frise, V. Kaynig, M. Longair, T. Pietzsch, S. Preibisch, C. Rueden, S. Saalfeld, B. Schmid, J. Y. Tinevez, D. J. White, V. Hartenstein, K. Eliceiri, P. Tomancak, and A. Cardona. 2012. 'Fiji: an open-source platform for biological-image analysis', *Nat Methods*, 9: 676-82.

64. Segall, J. E. 1993. 'Polarization of yeast cells in spatial gradients of alpha mating factor', *Proc Natl Acad Sci U S A*, 90: 8332-6.

65. Shimada, Y., M. P. Gulli, and M. Peter. 2000. 'Nuclear sequestration of the exchange factor Cdc24 by Far1 regulates cell polarity during yeast mating', *Nat Cell Biol*, 2: 117-24.

66. Slaughter, B. D., S. E. Smith, and R. Li. 2009. 'Symmetry breaking in the life cycle of the budding yeast', *Cold Spring Harb Perspect Biol*, 1: a003384.

67. Smith, G. R., S. A. Givan, P. Cullen, and G. F. Sprague, Jr. 2002. 'GTPase-activating proteins for Cdc42', *Eukaryot Cell*, 1: 469-80.

68. Sriram K., and P.A. Insel. 2018. 'G Protein-Coupled Receptors as Targets for Approved Drugs: How Many Targets and How Many Drugs?', *Mol Pharmacol*. 93:251–258.

69. Storici, F., and M. A. Resnick. 2006. 'The delitto perfetto approach to in vivo site-directed mutagenesis and chromosome rearrangements with synthetic oligonucleotides in yeast', *Methods Enzymol*, 409: 329-45.

70. Takizawa, P. A., J. L. DeRisi, J. E. Wilhelm, and R. D. Vale. 2000. 'Plasma membrane compartmentalization in yeast by messenger RNA transport and a septin diffusion barrier', *Science*, 290: 341-4.

71. Tanaka, H., and T. M. Yi. 2010. 'The effects of replacing Sst2 with the heterologous RGS4 on polarization and mating in yeast', *Biophys J*, 99: 1007-17.

72. Tedford, K., S. Kim, D. Sa, K. Stevens, and M. Tyers. 1997. 'Regulation of the mating pheromone and invasive growth responses in yeast by two MAP kinase substrates', *Curr Biol*, 7: 228-38.

73. Venkatapurapu, S. P., J. B. Kelley, G. Dixit, M. Pena, B. Errede, H. G. Dohlman, and T. C. Elston. 2015. 'Modulation of receptor dynamics by the regulator of G protein signaling Sst2', *Mol Biol Cell*, 26: 4124-34.

74. Versele, M., K. Lemaire, and J. M. Thevelein. 2001. 'Sex and sugar in yeast: two distinct GPCR systems', *EMBO Rep*, 2: 574-9.

75. Vida, T. A., and S. D. Emr. 1995. 'A new vital stain for visualizing vacuolar membrane dynamics and endocytosis in yeast', *J Cell Biol*, 128: 779-92.

76. Wang, Y., and H. G. Dohlman. 2004. 'Pheromone signaling mechanisms in yeast: a prototypical sex machine', *Science*, 306: 1508-9.

77. Whitworth, K., M. K. Bradford, N. Camara, and B. Wendland. 2014. 'Targeted disruption of an EH-domain protein endocytic complex, Pan1-End3', *Traffic*, 15: 43-59.

APPENDIX A. MICROFLUIDICS DEVICE

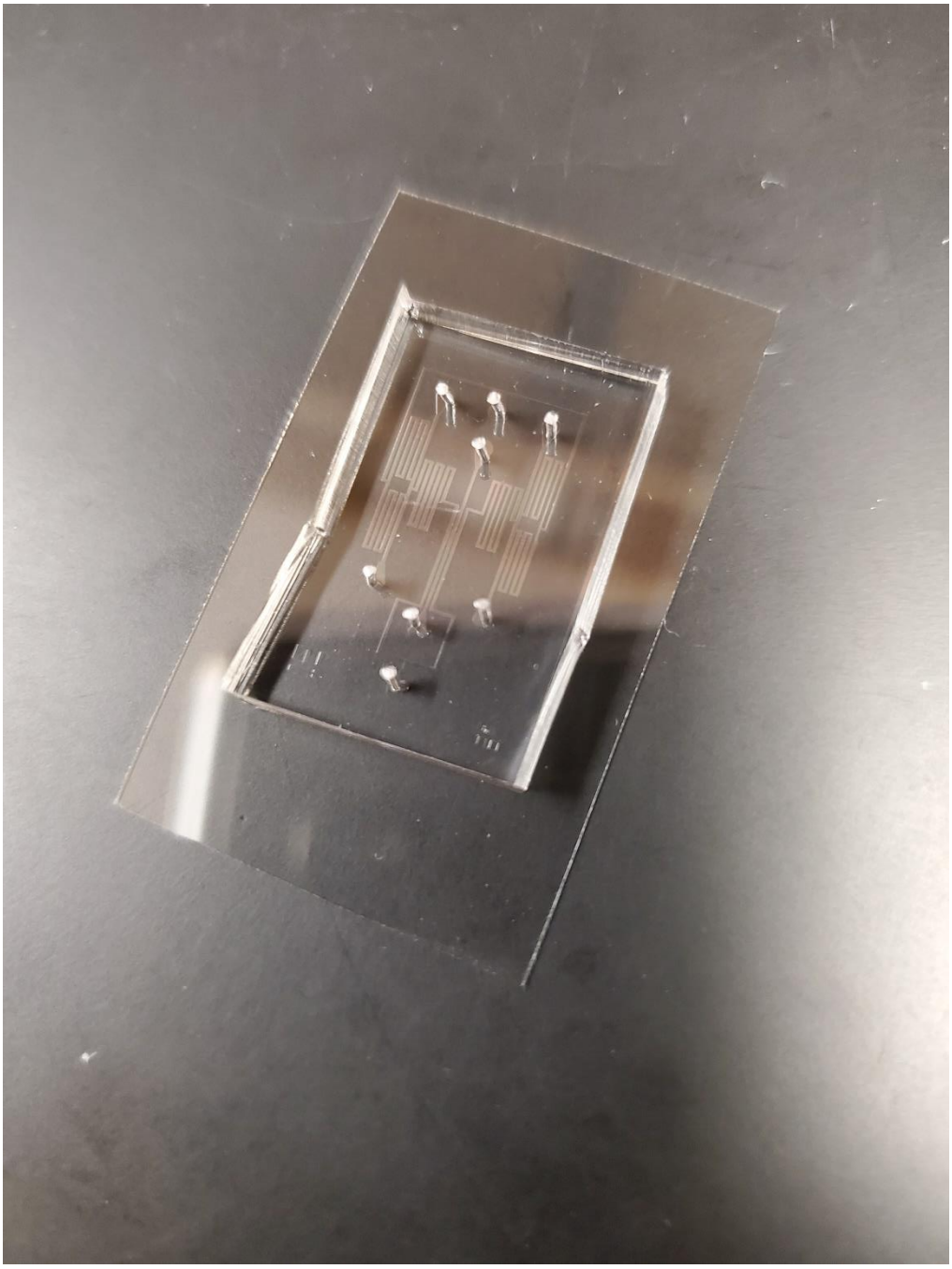

Figure A1. Image of Microfluidics Device

APPENDIX B. MATLAB NUCLEAR/VACUOLAR SUBTRACTION

```
maskcells = 'Cell Mask.tif';
maskdir = Nuclear_or_Vacuolar MASK.tif';
gfpdir = 'Fluorescent Protein of Interest.tif';

tmax =[];
tmax = 37;

for i = 1:tmax;
        preimin{i,1} = imread(maskdir,i);
        preimingfp{i,1} = imread(gfpdir,i);
        preiminma{i,1} = imread(maskcells,i);
end

x = size(preimin{1,1},2);
y = size(preimin{1,1},1);

for i = 1:tmax


            maskin{i,1} = preimin{i,1};
            gfpin{i,1} = preimingfp{i,1};
            cellmaskin{i,1} = preiminma{i,1};

            maskin{i,1} = ~maskin{i,1} > 0; %mask out of imagej
is inverted
            cellmask{i,1} = uint16(maskin{i,1});

            cellmaskin{i,1} = cellmaskin{i,1}./255;

            cellmask{i,1} = ~cellmask{i,1};
            cellmask2{i,1} = uint16(cellmask{i,1});

            Vacsub_gfp_im{i,1} = cellmask2{i,1}.*gfpin{i,1};
            Backsub_gfp_im{i,1} =
uint16(cellmaskin{i,1}).*gfpin{i,1};


            backsub_val{i,1} =
mean(mean(Backsub_gfp_im{i,1},1));
end

backmat = [];
backmat = cell2mat(backsub_val);
```

```
for i = 1:tmax
    for c = 1:x
        for d = 1:y
             if Vacsub_gfp_im{i,1}(d,c) ==0;
                 Vacsub_gfp_im{i,1}(d,c)= uint16(backmat(i,1));
             end
        end
    end

end

  imwrite(uint16(Vacsub_gfp_im{1,1}),'GFP_Sub.tif', 'WriteMode',
'OverWrite');

for i = 2:tmax;

imwrite(uint16(Vacsub_gfp_im{i,1}),'GFP_Sub.tif','WriteMode',
'append');
end
```

Figure B1. MATLAB Script to Remove Nuclear or Vacuolar Fluorescence

APPENDIX C. MATLAB ENDOCYTOSIS ALGORITHM

```
%% Find the mean endocytic rates over time looking at both the
mean internal fluorescence and the ratio of internal to membrane
bound

maskdir = 'tracked_mask.tif';
maskdirint = 'internal_mask.tif';
prot1dir = 'MAX_C2-
Pos1_11.14.18_sst2_s539d_gfp_synaptored_200nM_12hr_20min_int.tif
';
prot2dir = 'MAX_GFP_Pos1_11.14.18_Decon_7SNR.tif';

strain = ('S539D ')
prot1 = ('SynaptoRed ');
prot2 = ('Sst2-GFP ');

%%
preimin = cell(145,1);

tmin = 1;
tmax = [];
tmax = size(imfinfo(maskdir),1);
times = [tmin:1:tmax];

threshper = 99;
threshperl = 88;

maskin01 = [];
trackvar = [];

%% load images in
for c = 1:4
    if c == 1
        gadir = maskdir;
    elseif c==2
        gadir = prot1dir;
    elseif c == 3
        gadir = prot2dir;
    elseif c ==4
        gadir = maskdirint;

    end


    for i = 1:tmax
```

```
        preimin{i,1} = imread(gadir,i);
    end


    for i = 1:tmax
        if c ==1
            maskin{i,1} = preimin{i,1};
        elseif c == 2
            prot1in{i,1}= preimin{i,1};
        elseif c == 3
            prot2in{i,1}=preimin{i,1};
        elseif c ==4
            maskin_int{i,1} = preimin{i,1};
        end
    end
end

 figure();
 subplot(1,3,1), imagesc(maskin{tmax,1});
 subplot(1,2,1), imagesc(maskin{tmax,1});
 subplot(1,3,3), imagesc(prot2in{tmax,1});

tnum = tmax - tmin + 1;
max_field = zeros(tnum,1);
peak_thresh = cell(tmax,1);
currmax = [];
low_thresh_clean = cell(tnum,1);
low_thresh_count = zeros(tnum,1);
peak_thresh_count = zeros(tnum,1);
labeledmask_peak = cell(tnum,1);
labeledmask = cell(tnum,1);


%% Convert internal mask to MATLAB mask and find perimeter mask
for i = 1:tmax
    matmask{i,1} = ~maskin_int{i,1};
    dblmatmask{i,1} = uint8(matmask{i,1});
    labeledintmask = [];
    labeledintmask = dblmatmask{i,1}.*maskin{i,1};
    intmask{i,1} = labeledintmask;
    permask{i,1} = maskin{i,1}-intmask{i,1};
end
%% Find index of all pixels with each cell and the size of each
cell
cellnum = [];
cellnum = max(max(maskin{tmax,1}));
```

```
for i = 1:tmax %For Whole Cell
    for j = 1:cellnum
        currmask = [];
        currmask = maskin{i,1}==j;
        [ys,xs] = find(currmask);
        ind{i,j} = [ys,xs];
        cellsize(i,j) = size(ind{i,j},1);
    end
end

for i = 1:tmax %For Internal Only
    for j = 1:cellnum
        currmask = [];
        currmask = intmask{i,1}==j;
        [ys,xs] = find(currmask);
        indint{i,j} = [ys,xs];
        cellsizeint(i,j) = size(indint{i,j},1);
    end
end

for i = 1:tmax %For External only
    for j = 1:cellnum
        currmask = [];
        currmask = permask{i,1}==j;
        [ys,xs] = find(currmask);
        indext{i,j} = [ys,xs];
        cellsizeext(i,j) = size(indext{i,j},1);
    end
end
%% Find the GFP intensity at all pixels in exery cell, putting
this into a new variable

for i = 1:tmax % For whole cell
    for j = 1:cellnum
        for t = 1:cellsize(i,j)
            currind = [];
            currind = ind{i,j}(t,:);
            prot1val{i,j}(t,1) =
prot1in{i,1}(currind(1,1),currind(1,2));
            prot2val{i,j}(t,1) =
prot2in{i,1}(currind(1,1),currind(1,2));
        end
    end
end

for i = 1:tmax % For Internal Only
    for j = 1:cellnum
```

```
        for t = 1:cellsizeint(i,j)
            currind = [];
            currind = indint{i,j}(t,:);
            prot1valint{i,j}(t,1) =
prot1in{i,1}(currind(1,1),currind(1,2));
            prot2valint{i,j}(t,1) =
prot2in{i,1}(currind(1,1),currind(1,2));
        end
    end
end

for i = 1:tmax % For External Only
    for j = 1:cellnum
        for t = 1:cellsizeext(i,j)
            currind = [];
            currind = indext{i,j}(t,:);
            prot1valext{i,j}(t,1) =
prot1in{i,1}(currind(1,1),currind(1,2));
            prot2valext{i,j}(t,1) =
prot2in{i,1}(currind(1,1),currind(1,2));
        end
    end
end
%% Find the average value and fold change for each cell and for
all cells at every timepoint
meanprot1 = [];
singlecellmeanprot1 = [];
foldchangeprot1 = [];
meanprot2 = [];
singlecellmeanprot2 = [];
foldchangeprot2 = [];

for i = 1:tmax %For Whole Cell
    for j =1:cellnum

        if size(prot1val{i,j},1)>0
            singlecellmeanprot1(i,j) = mean(prot1val{i,j},1);
            foldchangeprot1(i,j) =
singlecellmeanprot1(i,j)/singlecellmeanprot1(1,j);
        else
            singlecellmeanprot1(i,j) = NaN;
            foldchangeprot1(i,j) = NaN;

        end

        if size(prot2val{i,j},1)>0
            singlecellmeanprot2(i,j) = mean(prot2val{i,j},1);
```

```
            foldchangeprot2(i,j) =
singlecellmeanprot2(i,j)/singlecellmeanprot2(1,j);
        else
            singlecellmeanprot2(i,j) = NaN;
            foldchangeprot2(i,j) = NaN;

        end
    end
end

meanprot1 = meannan(singlecellmeanprot1,2);
meanfoldchangeprot1 = meannan(foldchangeprot1,2);
for i = 1:tmax
    wholefoldprot1(i,1) = meanprot1(i,1)/meanprot1(1,1);
end

for i =2:tmax
    slopewholeprot1(i,1) = meanprot1(i,1)-meanprot1(i-1,1);
end

meanprot2 = meannan(singlecellmeanprot2,2);
meanfoldchangeprot2 = meannan(foldchangeprot2,2);
for i = 1:tmax
    wholefoldprot2(i,1) = meanprot2(i,1)/meanprot2(1,1);
end

for i =2:tmax
    slopewholeprot2(i,1) = meanprot2(i,1)-meanprot2(i-1,1);
end
%% Internal
meanprot1int = [];
singlecellmeanprot1int = [];
foldchangeprot1int = [];
meanprot2int = [];
singlecellmeanprot2int = [];
foldchangeprot2int = [];

for i = 1:tmax % For Internal Only
    for j =1:cellnum

        if size(prot1valint{i,j},1)>0
            singlecellmeanprot1int(i,j) =
mean(prot1valint{i,j},1);
            foldchangeprot1int(i,j) =
singlecellmeanprot1int(i,j)/singlecellmeanprot1int(1,j);
        else
            singlecellmeanprot1int(i,j) = NaN;
```

```
            foldchangeprot1int(i,j) = NaN;
        end

        if size(prot2valint{i,j},1)>0
            singlecellmeanprot2int(i,j) =
mean(prot2valint{i,j},1);
            foldchangeprot2int(i,j) =
singlecellmeanprot2int(i,j)/singlecellmeanprot2int(1,j);
        else
            singlecellmeanprot2int(i,j) = NaN;
            foldchangeprot2int(i,j) = NaN;
        end
    end
end
meanprot1int = meannan(singlecellmeanprot1int,2);
meanfoldchangeprot1int = meannan(foldchangeprot1int,2);
for i = 1:tmax
    wholefoldprot1int(i,1) =
meanprot1int(i,1)/meanprot1int(1,1);
end

for i =2:tmax
    slopeintprot1(i,1) = meanprot1int(i,1)-meanprot1int(i-1,1);
end

meanprot2int = meannan(singlecellmeanprot2int,2);
meanfoldchangeprot2int = meannan(foldchangeprot2int,2);
for i = 1:tmax
    wholefoldprot2int(i,1) =
meanprot2int(i,1)/meanprot2int(1,1);
end

for i =2:tmax
    slopeintprot2(i,1) = meanprot2int(i,1)-meanprot2int(i-1,1);
end
%% External
meanprot1ext = [];
singlecellmeanprot1ext = [];
foldchangeprot1ext = [];
meanprot2ext = [];
singlecellmeanprot2ext = [];
foldchangeprot2ext = [];
for i = 1:tmax %For Whole Cell
    for j =1:cellnum

        if size(prot1valext{i,j},1)>0
```

```
            singlecellmeanprot1ext(i,j) =
mean(prot1valext{i,j},1);
            foldchangeprot1ext(i,j) =
singlecellmeanprot1ext(i,j)/singlecellmeanprot1ext(1,j);
        else
            singlecellmeanprot1ext(i,j) = NaN;
            foldchangeprot1ext(i,j) = NaN;
        end

        if size(prot2valext{i,j},1)>0
            singlecellmeanprot2ext(i,j) =
mean(prot2valext{i,j},1);
            foldchangeprot2ext(i,j) =
singlecellmeanprot2ext(i,j)/singlecellmeanprot2ext(1,j);
        else
            singlecellmeanprot2ext(i,j) = NaN;
            foldchangeprot2ext(i,j) = NaN;
        end
    end
end

meanprot1ext = meannan(singlecellmeanprot1ext,2);
meanfoldchangeprot1ext = meannan(foldchangeprot1ext,2);
for i = 1:tmax
    wholefoldprot1ext(i,1) =
meanprot1ext(i,1)/meanprot1ext(1,1);
end

for i =2:tmax
    slopeextprot1(i,1) = meanprot1ext(i,1)-meanprot1ext(i-1,1);
end

meanprot2ext = meannan(singlecellmeanprot2ext,2);
meanfoldchangeprot2ext = meannan(foldchangeprot2ext,2);
for i = 1:tmax
    wholefoldprot2ext(i,1) =
meanprot2ext(i,1)/meanprot2ext(1,1);
end

for i =2:tmax
    slopeextprot2(i,1) = meanprot2ext(i,1)-meanprot2ext(i-1,1);
end

%% Find the ratio of Internal to external

ratiointtoextprot1 = [];
```

```
for i = 1:tmax
    for j = 1:cellnum

        ratiointtoextprot1(i,j) =
singlecellmeanprot1int(i,j)/singlecellmeanprot1ext(i,j);

    end
end

meanratio = meannan(ratiointtoextprot1,2);

ratiointtoextprot2 = [];

for i = 1:tmax
    for j = 1:cellnum

        ratiointtoextprot2(i,j) =
singlecellmeanprot1int(i,j)/singlecellmeanprot1ext(i,j);

    end
end

meanratio = meannan(ratiointtoextprot2,2);

%% Graph the values of mean gfp over time
figure()
subplot(2,2,1)
plot(meanprot1,'b', 'LineWidth', 3)
hold on
plot(meanprot2,'b:', 'LineWidth',3)
xlabel('Timepoint 20min int')
ylabel('Fluorescent Intensity')
title([num2str(strain),' Whole'])
legend([num2str(strain), num2str(prot1)],[num2str(strain),
num2str(prot2)])
hold off

subplot(2,2,2)
plot(meanfoldchangeprot1,'b', 'LineWidth', 3)
hold on
plot(meanfoldchangeprot2,'b:', 'LineWidth', 3)
xlabel('Timepoint 20min int')
ylabel('Fold Change Mean Individual')
title([num2str(strain),' Whole'])
legend([num2str(strain), num2str(prot1)],[num2str(strain),
num2str(prot2)])
hold off
```

```
subplot(2,2,3)
plot(wholefoldprot1,'b', 'LineWidth', 3)
hold on
plot(wholefoldprot2,'b:', 'LineWidth', 3)
xlabel('Timepoint 20min int')
ylabel('Fold Change Mean')
title([num2str(strain),' Whole'])
legend([num2str(strain), num2str(prot1)],[num2str(strain),
num2str(prot2)])
hold off

subplot(2,2,4)
plot(slopewholeprot1,'b', 'LineWidth', 3)
hold on
plot(slopewholeprot2,'b:', 'LineWidth', 3)
xlabel('Timepoint 20min int')
ylabel('Slope')
title([num2str(strain),' Whole'])
legend([num2str(strain), num2str(prot1)],[num2str(strain),
num2str(prot2)])
hold off

%% Internal graphs
figure()
subplot(2,2,1)
plot(meanprot1int,'b', 'LineWidth', 3)
hold on
plot(meanprot2int,'b:', 'LineWidth', 3)
xlabel('Timepoint 20min int')
ylabel('Fluorescent Intensity')
title([num2str(strain),' Internal'])
legend([num2str(strain), num2str(prot1)],[num2str(strain),
num2str(prot2)])
hold off

subplot(2,2,2)
plot(meanfoldchangeprot1int,'b', 'LineWidth', 3)
hold on
plot(meanfoldchangeprot2int,'b:', 'LineWidth', 3)
xlabel('Timepoint 20min int')
ylabel('Fold Change Mean Individual')
title([num2str(strain),' Internal'])
legend([num2str(strain), num2str(prot1)],[num2str(strain),
num2str(prot2)])
hold off
```

```
subplot(2,2,3)
plot(wholefoldprot1int,'b', 'LineWidth', 3)
hold on
plot(wholefoldprot2int,'b:', 'LineWidth', 3)
xlabel('Timepoint 20min int')
ylabel('Fold Change Mean')
title([num2str(strain),' Internal'])
legend([num2str(strain), num2str(prot1)],[num2str(strain),
num2str(prot2)])
hold off

subplot(2,2,4)
plot(smooth(slopeintprot1,6),'b', 'LineWidth', 3)
hold on
plot(smooth(slopeintprot2,6),'b:', 'LineWidth', 3)
xlabel('Timepoint 20min int')
ylabel('Slope')
title([num2str(strain),' Internal'])
legend([num2str(strain), num2str(prot1)],[num2str(strain),
num2str(prot2)])
hold off
%% External graphs
figure()
subplot(2,2,1)
plot(meanprot1ext,'b', 'LineWidth', 3)
hold on
plot(meanprot2ext,'b:', 'LineWidth', 3)
xlabel('Timepoint 20min int')
ylabel('Fluorescent Intensity')
title([num2str(strain),' External'])
legend([num2str(strain), num2str(prot1)],[num2str(strain),
num2str(prot2)])
hold off

subplot(2,2,2)
plot(meanfoldchangeprot1ext,'b', 'LineWidth', 3)
hold on
plot(meanfoldchangeprot2ext,'b:', 'LineWidth', 3)
xlabel('Timepoint 20min int')
ylabel('Fold Change Mean Individual')
title([num2str(strain),' External'])
legend([num2str(strain), num2str(prot1)],[num2str(strain),
num2str(prot2)])
hold off

subplot(2,2,3)
plot(wholefoldprot1ext,'b', 'LineWidth', 3)
```

```
hold on
plot(wholefoldprot2ext,'b:', 'LineWidth', 3)
xlabel('Timepoint 20min int')
ylabel('Fold Change Mean')
title([num2str(strain),' External'])
legend([num2str(strain), num2str(prot1)],[num2str(strain),
num2str(prot2)])
hold off

subplot(2,2,4)
plot(slopeextprot1,'b', 'LineWidth', 3)
hold on
plot(slopeextprot2,'b:', 'LineWidth', 3)
xlabel('Timepoint 20min int')
ylabel('Slope')
title([num2str(strain), ' External'])
legend([num2str(strain), num2str(prot1)],[num2str(strain),
num2str(prot2)])
hold off
```

Figure C1. MATLAB Script to Analyze Endocytosis Ratio

BIOGRAPHY OF THE AUTHOR

Will Simke was born in Baltimore, Maryland on May 19, 1994. He was raised in Lutherville, Maryland and graduated from Dulaney High School. He attended the University of Maryland Baltimore County and graduated in May 2016 with a Bachelor's in Science with a degree in Biochemistry and Molecular Biology. He moved to Brewer, Maine in the Summer of 2016 and entered the graduate school of Molecular and Biomedical Sciences, with a focus in Biochemistry. After receiving his degree, Will moved to Durham, North Carolina to complete his PhD in Chemistry at the University of North Carolina, Chapel Hill. Will is a candidate for the Master of Science degree in Biochemistry from the University of Maine in August 2019.